Anatomic and transcriptomic characterization of the canola (*Brassica napus*) funiculus during seed development.

by

Ainsley Chan

A thesis submitted to the Faculty of Graduate Studies
at the University of Manitoba
in partial fulfillment of the requirements of the degree of

MASTER OF SCIENCE

Department of Biological Sciences
University of Manitoba
Winnipeg, Manitoba, Canada

ABSTRACT

Canola (*Brassica napus*) is a $19.3 billion industry for the Canadian economy annually, largely because of the demand for the oil derived from the seeds of this crop plant. Seed development and accumulation of important nutrients requires coordinated interactions between all seed regions, including the funiculus. The funiculus is a structure of the seed that serves as the only connection between the filial seed and the parent plant, yet its development and underlying transcriptional programs have not been explored. Using light and transmission electron microscopy, I completed an anatomical study of the funiculus over the course of development, from the mature ovule to the post-mature green seed stage. My results show that all three plant tissue systems of the funiculus undergo profound changes at the histological and ultrastructural level. To understand the programs that orchestrate these changes in the globular stage funiculus, I used laser microdissection coupled with RNA-sequencing. This produced a high-resolution dataset of the mRNAs present in each of the three tissue systems of the funiculus. Various clustering analyses and gene ontology term enrichment analysis identified several important biological processes associated with each tissue system. My data show that cell wall growth occurs in the epidermis, photosynthesis occurs in the cortex, and tissue proliferation and differentiation occurs in the vasculature. The importance of these processes in supporting overall seed growth and development is discussed, which can have profound implications in the genetic modification of the canola seed through manipulating the transcriptional activity of the funiculus.

ACKNOWLEDGMENTS

First and foremost, I must thank my wonderful supervisor, Dr. Mark Belmonte. You have guided and encouraged me through the completion of an undergraduate Honors and now a Master's thesis. The training and advice I have received over the course of many years (yes, it really has been that long!) of working with you have been invaluable to my professional and personal development.

Of course, the rest of the Belmonte Lab – including past, current, and affiliate members – is also deeply deserving of my sincerest gratitude for reasons that are far too numerous and tedious to list here. Specifically, I must thank Michael Becker, Deirdre Khan, Ian Girard, Jenna Millar, David Sytnik, Sam Lee, Oiza Atta, Sherry Mao, Dennis Drewnik, Sara Kost, and Trent Workman. You have all assisted me academically, technically, and/or in some other capacity that I consider instrumental to my success in the Belmonte Lab.

To my M. Sc. Thesis committee members, Drs. Dana Schroeder and Claudio Stasolla, thank you for your guidance and involvement throughout this entire process. Many more thanks go out to those who have provided technical training or assistance, and/or use of laboratory materials or services for my project: André Dufresne, Dr. Michael Sumner, Dr. Cynthia Ellison, Aaron John Gartner, Dr. Jeffery Marcus, Julie Pelletier (from Dr. John Harada's lab), Mike Shaw, Dr. Isobel Parkin, and Christian Naguit.

I must also thank NSERC and the University of Manitoba (specifically, the Faculty of Graduate Studies, the Faculty of Science, and the Department of Biological Sciences) for making this opportunity a possibility for me at all. And finally, a tremendous and heartfelt thank you to

all my close friends and family for your sympathy, patience, and support throughout this entire

process and beyond!

TABLE OF CONTENTS

LIST OF TABLES

LIST OF FIGURES

LIST OF NON-COMMON ABBREVIATIONS USED

AGI   Arabidopsis Genome Initiative

DAP   days after pollination

DER   diglycidyl glycol ether of polypropylene

DESeq   differential expression of RNA-seq data at the gene level

DP   dominant pattern

ERL   vinylcyclohexene dioxide

FPKM   fragments per kilobase of exon per million mapped reads

FKM   fuzzy K means

GO   gene ontology

HSD   honestly significant difference

LMD   laser microdissection

NSA   nonenyl succinic anhydride

PAS   periodic acid-Schiff's

PCA   principal component analysis

PCD   programmed cell death

RC   raw count

RIN   RNA integrity number

RNA-seq   RNA sequencing

sRAP   simplified RNA-seq analysis pipeline

TBO   toluidine blue O

TEM   transmission electron microscropy/micrograph

TF   transcription factor

TUNEL   terminal dUTP nick and labeling

VLCFA   very-long-chain fatty acid

WF   whole funiculus

BACKGROUND AND RELEVANCE

Seeds are an essential part of the life cycle of higher plants because they are the progenitor to the next sporophytic generation. Canola (*Brassica napus*) is a flowering plant, meaning that the seeds originate from structures of the ovule. The ovule consists of the haploid megagametophyte (Harada et al. 2010) enclosed by the integuments, which are of parental sporophytic origin (Wan et al. 2002), and the funiculus, which connects the ovule to the placenta of the plant. Following a double fertilization event, the ovule undergoes major changes to become the embryo-bearing seed.

In several plant systems, seed development occurs in two phases: morphogenesis, followed by maturation (Belmonte et al. 2013). In the Brassicaceae, during morphogenesis, the zygote undergoes mitosis and eventually forms the globular embryo, the stage at which the first tissue is present (Harada et al. 2010). Major patterning of the embryo – whereby the root-shoot axis is defined, the apical meristems are formed, and all embryonic tissue layers are established – occurs by the heart stage (Harada et al., 2010). In these morphogenic stages, the nutrition provided by the parent plant is utilized for developmental processes (Gómez et al. 2006). During maturation, further increases in seed size are largely associated with cell enlargement and filling (Gutierrez et al. 2007; Harada et al. 2010). Nutrient reserves accumulate within the seed, starting with the deposition of starch granules, followed by proteins and lipids (Harada et al. 2010). It is these nutrients that are of particular interest to humans. Understanding the mechanisms concerting seed development provides the basic information from which new techniques can be engineered to influence seed development. This approach can allow us to manipulate plants to produce more seeds or seeds containing higher levels of compounds of interest.

Concurrent with embryo development, other tissues of the seed also change. The endosperm arises from another fertilization event between a sperm cell with the central nuclei of the mature megagametophyte (Huang et al. 2009). The resultant triploid cell first undergoes a number of syncytial divisions, generating a single multinucleate cell, which then undergoes cellularization – a series of cytoplasmic divisions (Berger 2003). The seed coat develops from the ovule integuments after fertilization, and serves to protect the embryo throughout seed dormancy until conditions are suitable for germination (Haughn and Chaudhury 2005). Although the embryo, endosperm, and seed coat have been studied extensively in canola and other species, the fourth compartment, the funiculus, has been largely neglected in the literature.

Seeds represent a large proportion of the daily calories consumed by humans (Hills 2004). Oilseeds, such as canola (*Brassica napus*) are especially valuable from a nutritional and economic perspective. Canola represents an enormous industry in Canada: it is the highest grossing cash crop, generating $19.3 billion to the Canadian economy in 2013, with approximately 18% of that sum (approximately $3.4 billion) attributed to Manitoba (Canola Council of Canada 2014). Products from canola include canola meal, which can be used as a food source for cattle in dairy farming, and canola oil, which not only holds promise as a viable source of biodiesel, but is also a very prevalent dietary item.

In the past decade, canola has more than doubled its annual economic contribution and since 2001, the demand for canola meal, oil and raw seeds has generally increased (Canola Council of Canada 2014). Furthermore, over the next 7-10 years, it is predicted that approximately 50-75% more canola oil will need to be produced to fulfill a global demand for seed oil (Weselake et al. 2009). Because the most valuable products from canola are derived from the seeds, research aimed at optimizing seed production or quality would be beneficial both agriculturally and

economically. Extensive literature addressing many aspects of seed biology exists; However, one crucial part of the seed, the funiculus, has not received much attention in any plant model. Thus, uncovering the cellular and molecular features of the canola funiculus should provide useful information for the improvement of seed quality in the most economically important crop in Canada.

OBJECTIVES OF THIS RESEARCH

Because the embryo, endosperm and seed coat have been studied extensively, and shown to display dramatic cellular and molecular changes throughout seed development (Belmonte et al. 2013), I hope that by investigating the funiculus, I can acquire a better understanding of its role in supporting the developing seed. *Brassica napus* – specifically, the products derived from its seeds – represents one of the most economically important crops in Canada and one of the most important food sources in the world. Although much literature has been established about canola biology and the biology of other important crop plants, surprisingly, there is very little information available regarding the funiculus during seed development and its role in supporting seed growth. Insight about how the funiculus contributes to seed development can provide a preliminary framework from which new ways of improving seed quality and/or yield can be developed.

1. ANATOMICAL STUDY OF THE FUNICULUS

1.1. Question:

What anatomical changes occur in the funiculus post-fertilization at the light and electron microscope level over developmental time?

1.2. Hypothesis:

Because the seed enlarges and accumulates storage products over the course of development, I predict that there will be a concomitant increase in funiculus size to support seed growth. As the funiculus must convey nutrients to the seed, I hypothesize that the funiculus itself may be a sink for carbohydrates, proteins and lipids, so the levels and distribution of these compounds will

change over time. A corresponding change in cellular structure and tissue patterning should be apparent with these changes, especially considering that the other seed compartments undergo dramatic histological changes as they develop.

Because the seed expands as it develops and is an important sink in the plant (Stadler et al. 2005), I predict that the vasculature, particularly phloem tissue, will increase to fulfill the metabolic demands of the developing seed. Increase in the vascular supply would likely correspond to the heart stage of development as the most tissue patterning occurs during this stage (Mordhorst et al. 1997). The most histological changes in the funiculus will likely occur at this stage as well. I expect that the greatest ultrastructural changes will arise during the mature green stage as nutrients are being transported to and accumulated in the seed coat, endosperm and embryo. Overall, I expect that the changes observed in the developing funiculus will be directly related to providing the necessary functions conducive to successful seed development.

1.3. Relevance:

Understanding how the anatomy of the funiculus changes over the course of its lifecycle reveals important information about how this structure might support the seed, and will provide the necessary information upon which further studies can be designed.

2. GENETIC CONTROL OF BIOLOGICAL PROCESSES OCCURRING IN THE FUNICULUS

2.1. Question:

What transcripts are differentially accumulated between the different tissue systems of the funiculus? What are the biological processes controlled by these genes?

2.2. Hypothesis:

Different plant tissue systems are specialized to perform different functions in the plant. Therefore, I expect that different sets of mRNAs will be present in the various tissues that correspond to the development of the funiculus.

My results show that the funiculus can be divided into three tissue systems: 1) dermal 2) ground, and 3) vascular. The dermal tissue system serves to enclose and protect underlying plant tissues through imparting mechanical support (Ramsay and Glover 2005). I expect that mRNA accumulation related to cell wall synthesis would be high in this tissue layer. The ground tissue system functions in nutrient storage and occupying space between the dermal and vascular tissue systems. I predict that this may be the least genetically active layer, but that there may be some transcripts present for nutrient mobilization. Finally, the vascular tissue system is responsible for long-distance transport of substances throughout the plant body and for structural support. Given that the conducting cell types of xylem tissue are dead at maturity, I expect that most of the genetic activity will occur in the phloem and any other supporting tissues present in the vasculature (e.g. xylem parenchyma, procambial cells). As the only vascular link from the parental vascular network to the rest of the developing seed (Erdelská and Stintzing 2011) – and therefore serving an irreplaceable role in seed nourishment – I expect that the vascular tissue of the funiculus will represent the most diverse gene activity.

2.3. Relevance:

Examining differential mRNA accumulation among the different tissue systems at the globular stage in funiculus development enables a description of which biological processes are occurring at this stage. Essential seed genes can be identified that demonstrate how the funiculus participates in overall successful seed development. This in turn can have profound agricultural applications in terms of genetically modifying processes of interest to maximize seed utility

and/or output in canola, the most valuable crop plant in Canada.

   The two objectives of this research project will be treated as separate chapters in my thesis.

INTRODUCTION

In flowering plants, seeds originate from structures of the ovule and undergo dramatic morphological and anatomical changes over the course of the plant lifecycle. In several plant systems, seed development occurs in two phases: morphogenesis followed by maturation (Gutierrez et al. 2007). In general, tissue systems of the embryo are established during morphogenesis while storage products, such as oil and protein, tend to accumulate during the maturation phase in preparation for seed dormancy (Harada et al. 2010). Within these phases, there are several distinct stages of development named for the notable changes that occur in the embryo over time. Concurrent with changes occurring in the embryo, other seed compartments are also modified. Despite a large body of evidence showcasing anatomical features of other major seed parts, such as the embryo, endosperm, and seed coat, a comprehensive examination of funicular anatomy from a developmental perspective has yet to be conducted in seeds of the Brassicaceae. In addition, anatomical studies of funiculi in other plant models (e.g. Mawson et al. 1994; Endo 2012) are limited.

The funiculus connects the rest of the ovule and, later, the seed to the placenta of the ovary of the parent plant (Endress 2011; Erdelská and Stintzing 2011) and is the only vascular link between the two plant generations. In addition to supplying the ovule/seed through its vasculature, other roles of the funiculus have been identified: i) orienting the micropyle of the seed through ovule curvature as it develops so that the micropyle is situated next to the funiculus, which then allows for ii) guidance of the pollen tube over the funiculus and to the micropyle to promote successful fertilization (Chapman and Goring 2010; Endress 2011). However, the funiculus remains a poorly understood structure that likely plays an important role in supporting

8

the ovule/seed during the reproductive stages of the plant lifecycle and, thereby, controlling seed growth and development. Thus, understanding the cellular features of this dynamic and essential structure over developmental time should provide a unique opportunity for enhancing seed prosperity in the future.

Endress et al. (2011) described most funiculi as being short, but some plant taxa possess long funiculi, the Brassicaceae being one such example. Endo (2012), in an anatomical study of funiculi in the Leguminosae, found that the funiculi in this family all possess the three basic plant tissue systems: an outermost epidermis, an intermediate cortex and an internal vascular strand. The composition and organization of these tissues varies among different plant systems (Endo 2012; Mawson et al. 1994).

Development of tissue systems may also be accompanied by changes in ultrastructural features of the cell. The cell wall often restricts the physical dimensions of individual plant cells, and is deposited and modified (to accommodate cell enlargement) in a coordinated manner to maximize its strength (Steeves and Sussex 1996). Matrix components of the cell wall are produced and delivered by the endomembrane system, and are directed by the cytoskeleton (Szymanski and Cosgrove 2009). As a necessary and natural part of cell differentiation for some types of cells (e.g. tracheary elements in xylem), programmed cell death (PCD) occurs as a part of development to disassemble the cytoplasm (van Doorn et al. 2011). This process is characterized by many distinct cellular events, most notably autophagy, vacuolization and organelle degeneration, resulting in cytoplasmic clearance. PCD has been demonstrated to occur in several cell layers of the integuments as they mature into the seed coat in canola (Wan et al. 2002). It is possible that such cellular changes can be observed occurring in the funiculus, the other maternal seed compartment. During seed development, the funiculus may continue to

function as an irreplaceable part of the seed, changing according to the demands of the rest of the

seed, given that other seed compartments also change anatomically as the seed develops.

This study provides the first anatomical, histological and ultrastructural description of the

funiculus of *Brassica napus*. I describe the ontogeny and changes observed in the three tissue

systems of the funiculus from ovule fertilization through to seed maturation. I characterize

changes in cell wall thickening in the epidermis, cellular breakdown of the cortex, and

proliferation of the vasculature, and provide insight into the functions of these anatomical

features.

MATERIALS AND METHODS

1. PLANT MATERIALS AND GROWTH

Seeds of double haploid *Brassica napus* 'Topaz' plants (line DH4079, a wild-type strain) were planted in a peat-based medium (Sunshine Mix #1; Sun Gro Horticulture, Agawam, MA, USA) and grown in growth chambers under the following conditions: 22°C, 50-70% relative humidity and long day conditions (16 hours light, 8 hours dark -100-150 μm photons•m^{-2}•s^{-1}). The top two open flowers of each inflorescence were manually pollinated by gently swirling a small cylindrical paintbrush over the fertile floral whorls to collect the pollen from the stamens and transfer it to the stigma of the centrally-located carpel. The pedicles of the pollinated flowers were tagged with colored tape for silique collection at a later date. Whole flowers containing carpels with mature ovules and whole siliques containing seeds at the globular, heart, mature green, and post-mature green stages of development – corresponding to 7, 10, 28 and 35 days after pollination (DAP), respectively – were collected and processed for further analysis.

2. QUANTIFICATION OF FUNICULUS GROWTH

Carpels or siliques corresponding to the stages described previously were harvested, opened, and the carpel/silique valves separated from the replum. The seeds were then removed and the remaining replum with the funiculi still attached was viewed using a Leica M80 stereo microscope (Leica Microsystems, Wetzlar, Germany). Macrographs were taken using Leica Application Suite version 3.7 software (Leica Microsystems, Wetzlar, Germany) and analyzed with ImageJ version 1.44 software (National Institute of Health, Bethesda, MD, USA). Fifty funiculi were measured from each of the following stages: ovules and seeds 7, 10, 28, and 35

DAP.

2.1 Statistical tests

The medial length and width of each funiculus were measured. Mean values and standard errors of the data sets were calculated. The raw data values were inputted into JMP version 8.0.1 software (SAS Institute Inc., Cary, NC, USA) to test for significant differences. Separate analysis of variance (ANOVA) tests for each dimension (length and width) were used to determine the statistical difference in growth characteristics over developmental time. To determine if the difference in size between the different developmental stages was significant, a Tukey's honestly significant difference (HSD) post hoc test was used. A p value less than 0.05 was considered statistically significant.

3. LIGHT MICROSCOPY

3.1. Tissue processing

Tissues from the different stages of development were processed in separate glass vials with threaded lids, and followed the protocol outlined by Yeung and Saxena (2005).

3.1.1. Fixation

Carpels and siliques were cut transversely into small pieces before being fixed. With larger siliques, a portion of the valve wall was also removed to aid in penetration of the solutions used for tissue processing. Freshly cut tissues were fixed in a solution of 2.5% glutaraldehyde and 1.6% paraformaldehyde in 1X phosphate-buffered saline overnight at 4ºC.

3.1.2. Dehydration

Dehydration occurred over 3 days, beginning with replacing the fixative with methyl cellosolve the first day and storing the tissue at 4ºC overnight. The following day, the

12

methylcellosolve was replaced with 100% ethanol and dehydrated overnight at 4ºC. The next

day, the old ethanol was removed and replaced with fresh 100% ethanol and left at 4ºC

overnight.

3.1.3. Infiltration

Following dehydration, the tissues were gradually infiltrated by replacing the ethanol with a

graded Historesin (Leica Microsystems, Wetzlar, Germany) series: 1/3 Historesin, 2/3

Historesin, then 100% Historesin (x3 changes). Each day, the previous solution was exchanged

for the next solution in the series. Infiltration occurred in a rotary mixer at room temperature.

3.2. Embedding

After infiltration was complete, the tissues were embedded in a medium composed of the

following ratio: 91.5% Historesin, 2.4% polyethylene glycol 400 and 6.1% Historesin Hardener

(Leica Microsystems, Wetzlar, Germany). The tissues were placed in a mould plate with the

embedding solution, and left undisturbed overnight at room temperature to polymerize into solid

plastic blocks.

3.3. Sectioning and mounting

3 µm thick sections were produced from each block using disposable steel blades mounted

on a Leica RM2245 microtome (Leica Microsystems, Wetzlar, Germany). Ribbons of serial

sections were mounted on glass slides with distilled water. The slides were placed on a slide

warmer set to approximately 35-45ºC to dry completely prior to staining.

3.4. Staining

The sections were oxidized in 0.1% periodic acid for 15 minutes then stained with Schiff's

reagent for 15 minutes. After the periodic acid-Schiff (PAS) reaction, the slides were rinsed with

distilled water and then stained with toluidine blue O (TBO) in 0.1 mol•L^{-1} benzoate buffer for 1

minute. PAS reveals general insoluble carbohydrates as red or pink structures (Yeung and

Saxena 2005). TBO shows basic histological characteristics and serves as an excellent

counterstain to PAS (Yeung and Saxena 2005). TBO is a polychromatic dye that stains the pectic

acids of primary cell walls red or purple, the lignin of secondary cell walls blue, and phenolic

compounds blue-green (Yeung and Saxena 2005).

3.5. Imaging

Coverslips were applied to the dried slides using Cytoseal[TM] 60 (Richard-Allen Scientific,

Kalamazoo, MI, USA) as the adhesive medium. Slides were viewed using a brightfield light

microscope and micrographs were taken using Q capture pro software (QImaging, Surrey, BC,

Canada). The images were modified (cropped, addition of scale bars, contrast and brightness

adjusted, color balanced) with Adobe Photoshop CS2 version 9.0 software (Adobe Systems Inc.,

San Jose, CA, USA).

4. TRANSMISSION ELECTRON MICROSCOPY (TEM)

4.1. Tissue processing

As with the tissues for light microscopy, the tissues from the different stages of development

were processed in separate capped glass vials.

4.1.1. Fixation and post-fixation

Tissues for transmission electron microscopy were cut as described for light microscopy and

fixed in 3% gluteraldehyde in 0.025 mol•L^{-1} cacodylate buffer supplemented with 5 mmol•L^{-1}

CaCl$_2$ (pH 7.0) overnight at 4ºC. After fixation, the fixative was removed and the tissues were

rinsed with cacodylate buffer 3x and left in a rotary mixer at room temperature for 5 minutes

after each rinse. The tissues were then post-fixed in a solution of 2% OsO$_4$ and 0.8% KFe(CN)$_6$

in cacodylate buffer overnight at 4ºC.

4.1.2. In-block staining

The next day, the tissues were rinsed with distilled water 3x then left in distilled water and placed in a rotary mixer at room temperature for 1 hour. Following this hour, the tissues were rinsed another 3x with distilled water then stained overnight with a 0.5% uranyl acetate solution at 4ºC.

4.1.3. Dehydration

The following day, the tissues were again rinsed with 3 changes of distilled water, placed in a rotary mixer at room temperature for 1 hour, then rinsed again with 3 changes of distilled water.

Dehydration occurred using a graded ethanol series (35%, 50%, 70%, 95% [x2], 100% ethanol [x3]), remaining in each solution in the series for approximately 30 minutes at 4ºC (the tissue can be stored in ≥70% ethanol for longer periods of time [e.g. overnight]). After the third change of 100% ethanol, the tissues were left at 4ºC overnight. The next day, the ethanol was replaced with a fresh change of 100% ethanol for 30 minutes at 4ºC. The ethanol was then replaced with a 1:1 (*v/v*) ratio of 100% ethanol-propylene oxide solution for 15 minutes, followed by 3 changes of 100% propylene oxide, remaining in each rinse for 10-15 minutes. All dehydration phases involving propylene oxide were carried out at room temperature.

4.1.4. Infiltration

Spurr's epoxy resin was used to infiltrate the tissues. To make 20 mL of the resin, 5 g of vinylcyclohexene dioxide (ERL) 4206, 3 g of diglycidyl glycol ether of polypropylene (DER) 736 and 13 g of nonenyl succinic anhydride (NSA) were combined. To make the resin with activator (hardener), 0.2 g S-1 epoxy sealer was added to the above recipe. The resin was stirred thoroughly before each use with a magnetic stir bar on a magnetic plate.

After dehydration, the propylene oxide was replaced with a 1:1 (*v/v*) ratio of propylene oxide:resin (without activator) and left in a rotary mixer at room temperature overnight. A change of 100% resin followed the next day and the samples were returned to and remained in the rotary mixer overnight. Twice daily (once at the beginning and once at the end, to prevent premature polymerization), for the next two days, the old resin was replaced with fresh resin with activator.

4.2. Embedding

Following infiltration, the tissues were embedded in small aluminum pans with the resin with activator. The pans were then placed in a 70ºC oven overnight to polymerize the resin. The aluminum was peeled off each resulting resin disc. Blocks were sawed out of the disc and mounted on resin stubs.

4.3. Sectioning and mounting

Ultrathin sections (approximately 70 nm thick) were cut with a diamond knife (Drukker International) on a Reichert-Jung Stereo Star Zoom ultramicrotome (Reichert Technologies, Depew, NY, USA) and mounted on copper mesh grids.

4.4. Imaging

Grids bearing the sections were examined using a Hitachi H 7000 transmission electron microscope (Hitachi Ltd., Tokyo, Japan) at 75V. The transmission electron micrographs (TEMs) were taken using AMT Image Capture Engine version 601.384 software (Advanced Microscopy Techniques, Corp., Woburn, MA, USA) and modified (cropped, addition of scale bars, contrast and brightness adjusted, color balanced) using Adobe Photoshop CS2 version 9.0 software (Adobe Systems Inc., San Jose, CA, USA).

RESULTS

1. GROWTH OF THE CANOLA FUNICULUS THROUGHOUT DEVELOPMENT

In canola, developing ovules and seeds are anchored to the replum (placenta) via the funiculus (Figure 2.1A-E). The ovules and early seeds are relatively transparent (Figure 2.1A-C), whereas the mature seeds are notably full and green or brown (Figure 2.1D, E). Conversely, the funiculus begins as a densely green structure (Figure 2.1A-C), but as the seed develops, the funiculus color changes to a pale yellow (Figure 2.1D, E).

Concomitant with the increase in seed size over developmental time, the funiculus also increases in size from the ovule to the post-mature green stage of development (Figure 2.1F, G), with the length increasing 626% and the width increasing by 460% between these two stages. According to an ANOVA test, the change in funiculus length over developmental time was significantly different ($p < 0.0001$) and a Tukey's HSD post hoc test revealed that the difference in funiculus length was significant between all the stages (Figure 2.1F). Likewise, an ANOVA test showed that funiculus width changed significantly over the course of development ($p < 0.0001$) and a Tukey's HSD post hoc test demonstrated that the difference in width was significant between all stages as well (Figure 2.1G).

2. ANATOMICAL CHANGES IN THE CANOLA FUNICULUS THROUGHOUT DEVELOPMENT

To better understand changes in funiculus growth, I then performed a comprehensive anatomical analysis of this dynamic structure. The funiculus of canola is composed of the outermost single-cell-layered epidermis, a central collateral vascular bundle, and a ground tissue

17
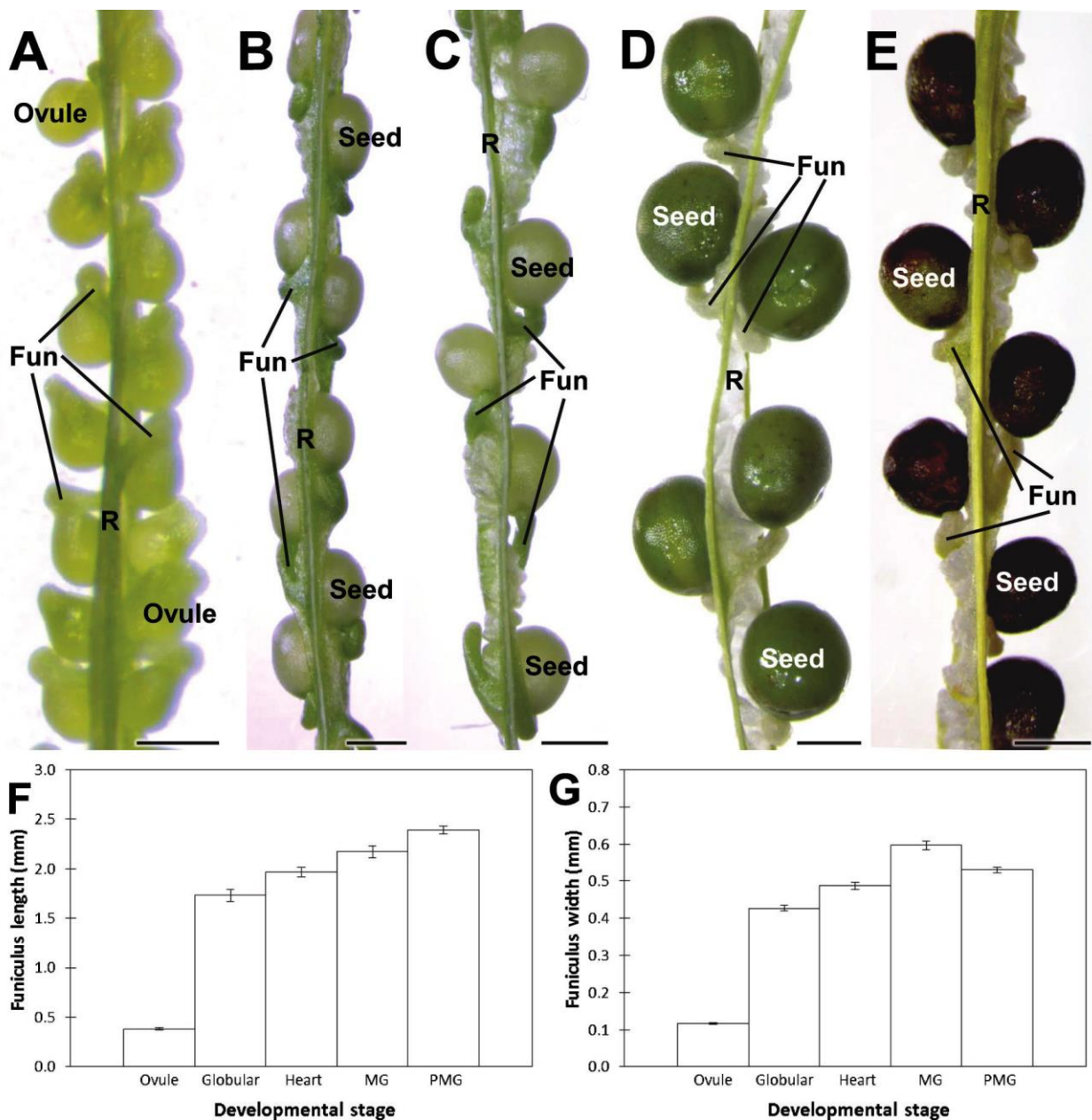
Figure 2.1: *Brassica napus* carpel (A) and globular (B), heart (C), mature green (D), and post-mature green (E) stage silique dissections. R = replum; Fun = funiculus; MG = mature green; PMG = post-mature green. The mean (± standard error) length (F) and width (G) of the funiculus changes over developmental time. According to ANOVA and Tukey's HSD post hoc tests, the changes in length and width are significantly different between all stages (n = 50). Scale bars: A = 0.60 mm; B = 1.40 mm; C = 1.40 mm; D = 1.35 mm; E = 1.60 mm.

composed of parenchyma cells found between the vascular strand and the epidermis. These

tissue systems persist throughout seed development, but undergo dramatic changes (Figure 2.2).

Figures 2.2-2.5 show the changes in canola funiculi as they develop from the mature ovule stage

through to the mature seed and will be described in terms of how each tissue system changes.

2.1. Epidermis

At the light microscope level, new cell wall formation in the radial plane can be observed in

the epidermis at the ovule and globular stages (Figure 2.2A, C). This is accompanied with cell

enlargement, increasing the circumference of the funiculus to accommodate the increasing girth

of the funiculus throughout development. Later in development, the cell walls of the epidermis

thicken, particularly the periclinal walls and especially the outer wall. This first appears in the

globular stage but is more notable in later stages (Figure 2.2). However, the cell wall remains

primary throughout development as revealed by the deep purple color of the TBO stain.

Vesicular activity is abundant throughout the morphogenesis phase (Figure 2.3C, E, F). The

undulating border of the cytoplasmic surface of the cell wall and its proximity to vesicles

suggests recent vesicular fusion in cell wall formation in young stages (Figure 2.3E).

Intact nuclei are present during seed morphogenesis, but begin degrading at the heart stage,

as indicated by chromatin fragmentation (Figure 2.3G). By the mature green stage, intact nuclei

are rare, and by the post-mature green stage, they are non-existent. In early development,

chloroplasts contain intact grana and large, often compound, starch grains (Figure 2.3A, B, D).

As with nuclei, chloroplasts begin degenerating at the heart stage. Electron-dense plastoglobuli

begin to appear and starch is reduced (Figure 2.3H). During the seed maturation phase, the

cytoplasm displays clear signs of breakdown and is very indistinct (Figure 2.3I). By the post-

mature green stage, any remaining organelles are incorporated into the vacuole, which has
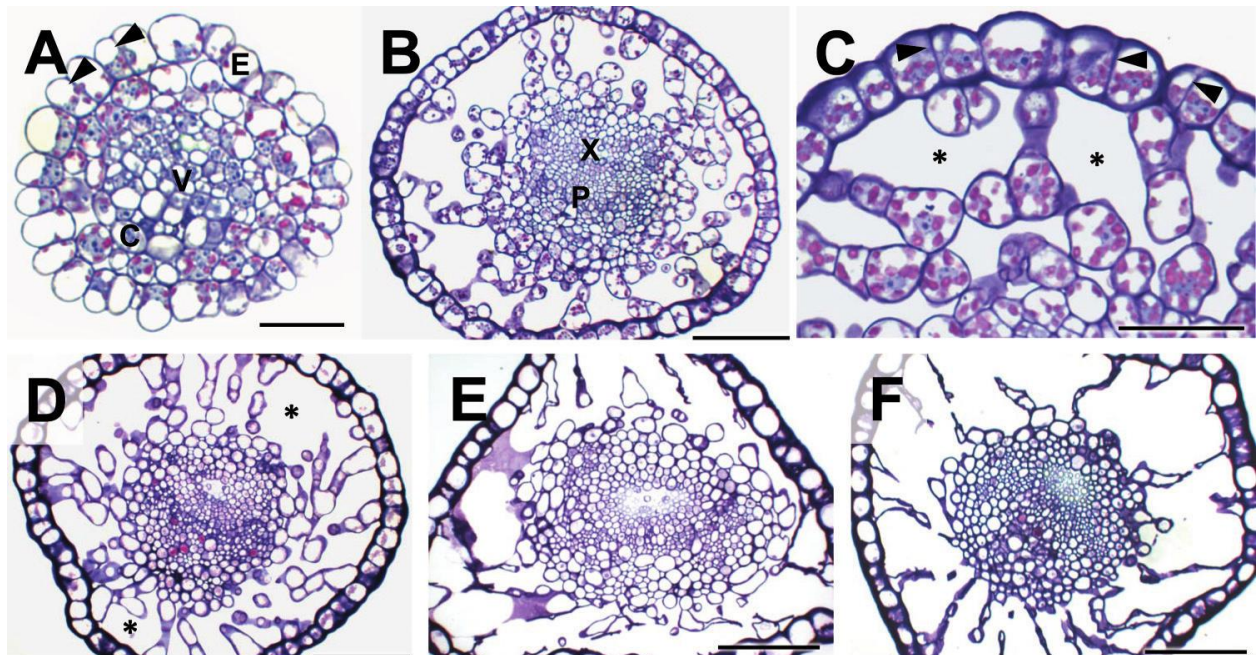
Figure 2.2: Light micrographs of 3 µm thick histological cross-sections of *Brassica napus* funiculi from various stages of seed development.

A: Mature ovule showing all three plant tissue systems: dermal (epidermis, E), ground (cortex, C), and vascular (V). Anticlinal cell divisions (arrowheads) are evident in the epidermis layer. These and the tightly packed cortex layer are abundant in starch (magenta from PAS reaction). Scale bar = 35 µm.

B: Globular seed (7 DAP) showing xylem (secondary cell walls blue from TBO staining, X) and phloem (P) development relative to the ovule. Scale bar = 105 µm.

C: Epidermis and cortex of globular (7 DAP) seed. Anticlinal divisions (arrowheads) are apparent in the epidermis, which is also exhibiting periclinal cell wall thickening (deep purple from TBO staining). Starch (magenta from PAS reaction) is present in the epidermis and cortex. The cortical cells are detaching from one another, leaving notable intercellular spaces (*). Scale bar = 35 µm.

D: Heart stage seed (10 DAP). Periclinal cell walls of the epidermis, and the intercellular spaces (*) in the cortex, which is vacuolating and breaking down, are enlarging. Starch is reduced (lack of magenta). Scale bar = 125 µm.

E: Mature green seed (28 DAP). Vacuolization is notable in both the epidermis and cortex. The epidermis' periclinal walls are even more thickened, particularly on the outer surface (deep purple from TBO staining). The cells of the cortex are collapsing, further increasing intercellular spaces in this tissue layer, although inner cortical cells are intact. The xylem and phloem of the vasculature has increased. Scale bar = 150 µm.

F: Post-mature green seed. Periclinal cell walls, especially the external surface, of the epidermis are even thicker than in younger stages (deep purple from TBO staining). The innermost cortical cells are intact but fully vacuolated, and only remnants of cell wall material remains of the outer cortical cells, producing large intercellular spaces in this layer. Xylem and phloem are extensive. Scale bar = 135 µm.

Figure 2.3: Transmission electron micrograph (TEM) of the epidermis from cross-sections of *Brassica napus* funiculi at various stages of seed development.
A: Whole epidermal cell from a mature ovule. The cytoplasm is intact with a nucleus (N) despite a large vacuole (Vac). Scale bar = 4 µm.
B: Chloroplast from a mature ovule showing starch grains (S) and intact thylakoid membranes arranged into granal stacks (*). Scale bar = 500 nm.
C: Mature ovule. Golgi (G) with vesicles (V) are proximal to a cell wall (CW). Scale bar = 200 nm.

D: Whole epidermal cell from a globular seed (7 DAP). Chloroplasts contain numerous starch grains (S) and the nucleus (N) is still intact. Vacuolar (Vac) expansion has occurred. Scale bar = 4 µm.

E: Globular seed (7 DAP). Golgi (G) and vesicles (V) are associated with the cell wall (CW), which has thickened. An inclusion (arrow) can be seen in the vacuole (Vac). Scale bar = 500 nm.

F: Whole epidermal cell from a heart stage seed (10 DAP). Starch (S) is still present and vesicular activity (V) is still extensive. The vacuole (Vac) contains inclusions (arrow). Scale bar = 8 µm.

G: Nucleus (N) from a heart stage seed (10 DAP) exhibiting signs of degradation. Chromatin fragments (Chr) are evident. Scale bar = 2.5 µm.

H: Heart stage seed (10 DAP). Chloroplasts still retain some starch (S) although they are breaking down. Plastoglobuli (small white arrows) are present and thylakoid membranes are indistinct. The vacuole (Vac) has inclusions (arrow). Scale bar = 500 nm.

I: Whole epidermal cell from a mature green seed (28 DAP). Cytoplasm is reduced and indistinct because of advanced degradation. The vacuole (Vac) constitutes the majority of the cell volume. Scale bar = 8 µm.

J: Whole epidermal cell from a post-mature green seed (35 DAP). The cell is entirely vacuolated (Vac) and the contents are entirely homogenous except for the most recently integrated parts of the cytoplasm, forming vacuolar inclusions (arrows). Scale bar = 8 µm.

K: A close-up of Figure 2.3J. Vacuolar inclusions are deteriorating within the vacuole (Vac) of the cell. CW = cell wall. Scale bar = 1 µm.

completely overtaken the cytoplasm (Figure 2.3J). Numerous inclusions are evident in the vacuole throughout development, but the vacuolar contents appear more uniform in the post-mature green stage (barring, of course, the most recent inclusions) (Figure 2.3K), suggesting degradation of those contents over developmental time.

2.2. Cortex

The cortex in the ovule is composed of a few layers of parenchyma cells encircling the vascular strand (Figure 2.2A), but after fertilization it expands to be several cell layers thick. This growth would be caused by periclinal divisions to enlarge the funiculus radially. However, proliferation of the cortical cells in the anticlinal plane appears to occur at a rate that is much slower than that of the periclinal divisions. Eventually all divisions cease and the cortex does not enlarge proportionally with the rest of the funiculus. As a result of the uneven division rates, intercellular spaces begin to appear in the cortex by the globular stage (Figure 2.2B). Because the rest of the funicular tissues exhibit continuous growth throughout development, the cortex parenchyma transitions from being tightly packed to loosely distributed to fill the intermediate space between the epidermis and the vascular strand. At the globular stage, the cortical cells are still largely intact, but by the end of morphogenesis and throughout maturation, the cells become vacuolated and collapse and eventually only remnants of cell walls remain (Figure 2.2B, D-F). This degradation occurs in the peripheral cortex first whereas the innermost cells immediately outside the vascular strand remain intact but still become highly vacuolated (Figure 2.2B, D-F).

Many large starch grains can be found within fully formed and functional chloroplasts at the ovule and globular stage (Figure 2.4A-C). By the heart stage, the chloroplasts appear notably degraded with indistinct thylakoids, reduced starch, and the development of plastoglobuli (Figure 2.4G). As observed at the light level (Figure 2.2D), the cells proximal to the vasculature are more

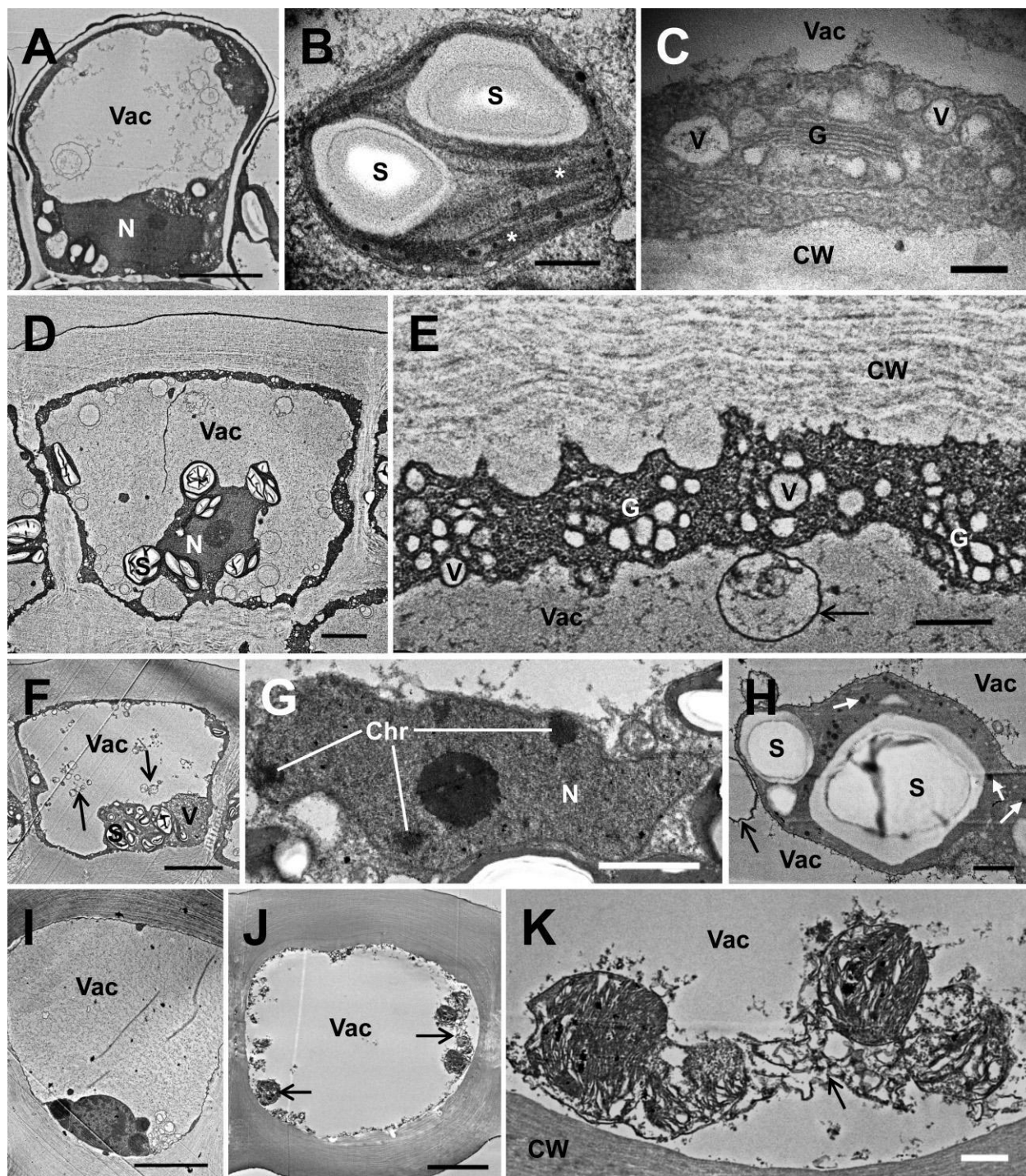**Figure 2.4:** Transmission electron micrograph (TEM) of the cortex from cross-sections of *Brassica napus* funiculi at various stages of seed development.

A: Whole cortical cell from a mature ovule showing vacuoles (Vac) and chloroplasts with large compound starch grains (S). Scale bar = 2.5 μm.

B: Chloroplast from a mature ovule showing intact thylakoid membranes arranged into granal stacks (*) and starch grains (S). Scale bar = 700 nm.

C: Whole cortical cell from a globular seed (7 DAP). The cell is intact with a distinct nucleus (N) and abundant starch (S) in chloroplasts. The vacuole (Vac) is beginning to develop inclusions (arrow). Scale bar = 4 μm.

D: Whole cortical cell from a heart stage seed (10 DAP) near the vasculature. The cytoplasm is intact with a nucleus (N), chloroplasts with starch (S), and a vacuole (Vac). Scale bar = 3 μm.

E: Whole cortical cell from a heart stage seed (10 DAP) near the epidermis. The cell is largely vacuolated (Vac) and contains inclusions (arrow), and cytoplasm is reduced. Scale bar = 2 μm.

F: Heart stage seed (10 DAP) showing chromatin fragmentation (Chr) in the nucleus (N). Vac = vacuole. Scale bar = 1.5 μm.

G: Heart stage seed (10 DAP). Chloroplasts lack distinct thylakoid membranes and possess plastoglobuli (small white arrows). Starch (S) is reduced. M = mitochondrion. Scale bar = 500 nm.

H: Whole cortical cell from a mature green seed (28 DAP). Cytoplasm is reduced and pushed to the periphery of the cell and the vacuole (Vac) with inclusions (arrows) occupies most of the space. Scale bar = 2 µm.

I: Mature green seed (28 DAP). A mitochondrion (M) is exhibiting signs of degeneration, including numerous osmophilic bodies (Os). This mitochondrion has been consumed by the vacuole (Vac), which has other inclusions (arrow). CW = cell wall. Scale bar = 200 nm.

J: Whole cortical cell from a post-mature green seed (35 DAP). This cell is entirely vacuolated (Vac), and its contents are homogenous. Scale bar = 4 µm.

cytoplasmically dense and intact (Figure 2.4D), whereas the cells closer to the epidermis are

more vacuolated and have more degenerated cytoplasms (Figure 2.4E). The nucleus, which was

intact in the previous stages (Figure 2.4C), displays chromatin fragmentation in the heart stage

(Figure 2.4F) and is absent throughout maturation. In the mature green stage, organelle integrity

has deteriorated so much that only mitochondria are recognizable despite containing multiple

osmiophilic bodies and clearly also being in the late stages of disintegration (Figure 2.4I). In

mature seeds, any remaining cortical cells are entirely vacuolated, or nearly so (Figure 2.4H, J),

and the progressive homogeneity of the vacuole lumen, most notably at the post-mature green

stage (Figure 2.4J), suggests complete lysis of its contents.

2.3. Vascular Strand

The central vascular cylinder dramatically increases in size from the ovule to mature stages

of funicular development. In the ovule, the vascular strand is small. Phloem composes the

majority of the vasculature and very few tracheary elements are present (Figure 2.2A). Following

fertilization, the vascular tissue quickly becomes notably larger. This is because of an increased

number of cells, not cell enlargement. Both xylem and phloem increase, although phloem

remains more abundant throughout development (Figure 2.2). During morphogenesis, the

amount of phloem far exceeds that of xylem, but in the maturation phase, xylem increases so that

the proportion of the two vascular tissues is more equal (Figure 2.2). The phloem tissue is packed

throughout development (Figure 2.2), but in the xylem, intercellular spaces occur between

tracheary elements, particularly toward the end of seed development (Figures 2.2E, 2.5B).

The general morphology of the tracheary elements remains consist throughout seed

development: noticeable deposits of secondary cell wall are found toward the central lumen

(Figure 2.5A). Differentiating tracheary elements can be observed. These cells have the

distinctive secondary wall morphology of mature tracheary elements but also contain some

degrading cytoplasm (Figure 2.5A). Tracheary elements tend to be small with a high cell wall to

lumen ratio.

TEM images reveal that the phloem tissue in the mature ovule is highly parenchymatous

(Figure 2.5B). Few conducting cell types can be found and they are scattered throughout the

phloem region of the vascular bundle. By the end of morphogenesis, however, more sieve tube

elements and companion cells appear (Figure 2.5C) although the tissue still contains abundant

parenchyma. During the maturation phase, the phloem becomes crushed and the cells are heavily

vacuolated (Figure 2.5D, E) with multiple inclusions found in vacuoles of the phloem cells at the

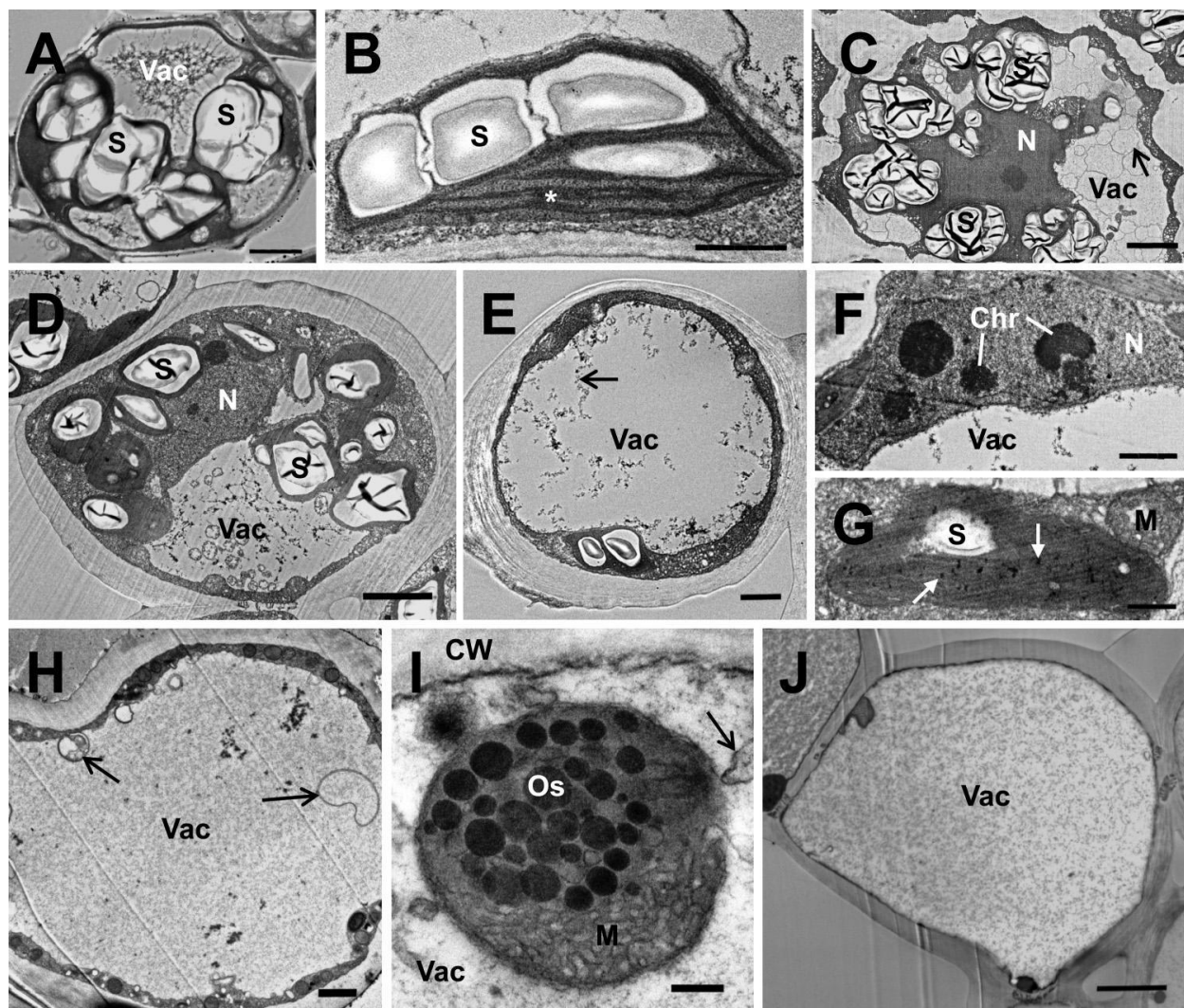post-mature green stage (Figure 2.5E).
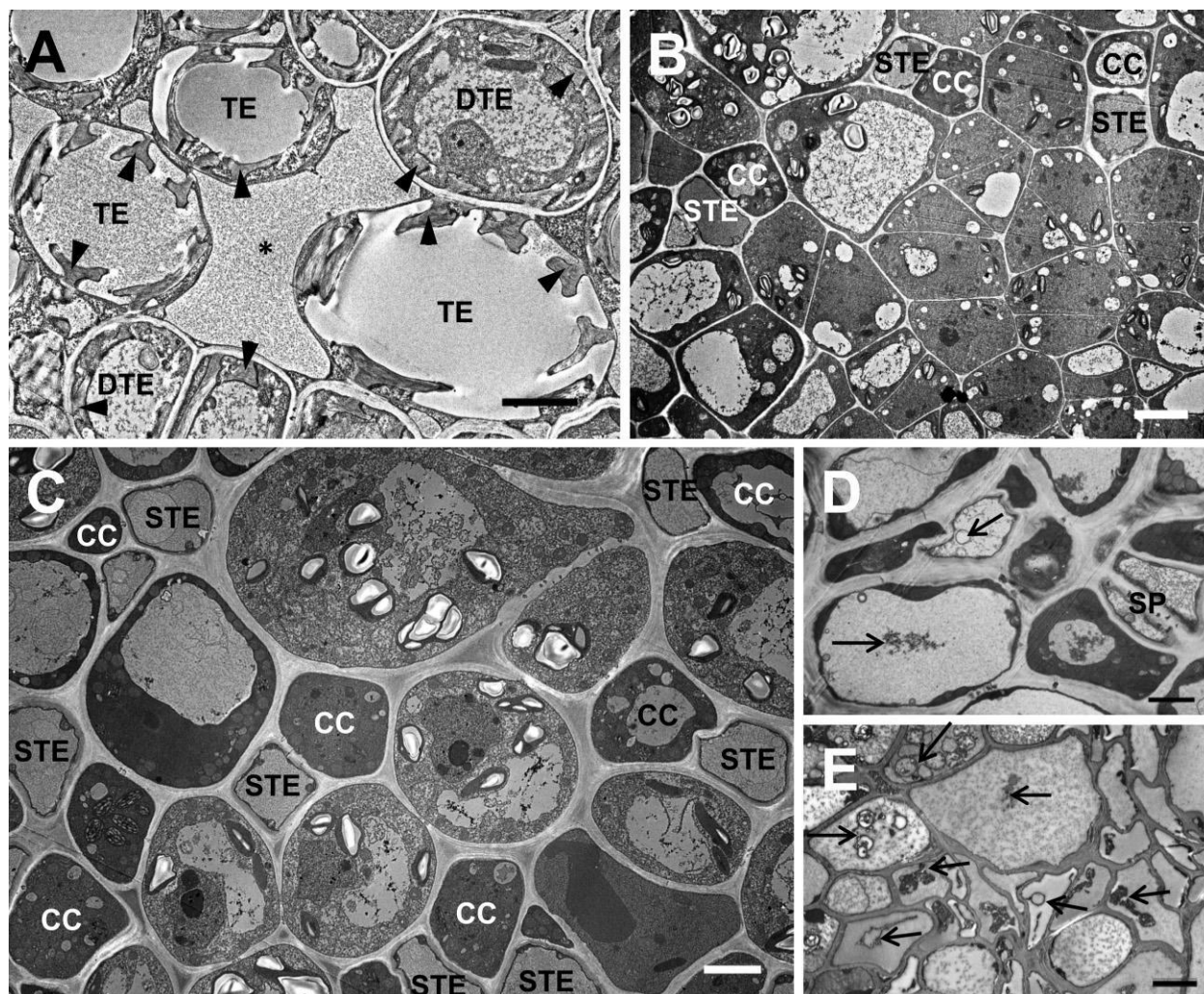
Figure 2.5: Transmission electron micrograph (TEM) of the vasculature from cross-sections of *Brassica napus* funiculi at various stages of seed development.

A: Xylem tissue from a heart stage seed (10 DAP). Arrowheads indicate secondary cell wall deposition in tracheary elements (TE). Developing tracheary elements (DTE) are evident as they have the characteristic secondary cell walls, but have yet to lose their cytoplasm. Intercellular spaces (*) are present in this tissue. This TEM image is representative of xylem tissue throughout seed development. Scale bar = 4 µm.

B: Phloem tissue from a mature ovule. Sieve tube elements (STE) and companion cells (CC) are few and scattered among parenchyma tissue. Scale bar = 4 µm.

C: Phloem tissue from a heart stage seed (10 DAP). There are more sieve tube elements (STE) and companion cells (CC) per surface area than in younger seeds. Scale bar = 4 µm.

D: Phloem tissue from a mature green seed (28 DAP). Cells are deforming and becoming more vacuolated with vacuolar inclusions (arrows). SP = sieve plate. Scale bar = 2.5 µm.

E: Phloem tissue from a post-mature green seed (35 DAP). Cells are entirely vacuolated with notable inclusions (arrows) and are collapsing. Scale bar = 6 µm.

Table 2.1: Summary of major features in the plant tissue systems of *Brassica napus* funiculi throughout seed development.

Stage	Epidermis	Cortex	Vasculature
Mature ovule	Thin-walled cells Anticlinal divisions Starch in chloroplasts Nucleus present	Cell layers packed Starch in chloroplasts Nucleus present	Phloem area relatively large Xylem rare Tracheary elements with uniformly thickened 2º walls
Globular seed (7 DAP)	Thick cell walls Anticlinal divisions Vesicular activity Starch in chloroplasts Nucleus present	Intercellular spaces Starch in chloroplasts Nucleus present	Xylem proliferation Phloem proliferation Tracheary elements with non-uniformly thickened 2º walls
Heart seed (10 DAP)	Thick cell walls Vesicular activity Starch reduction Chloroplast degeneration* Nuclear breakdown* Vacuolization*	Intercellular spaces Starch reduction Chloroplast degeneration* Nuclear breakdown* Vacuolization*	Xylem proliferation Phloem proliferation Tracheary elements with non-uniformly thickened 2º walls
Mature green seed (28 DAP)	Thick cell walls Chloroplast degeneration* Nuclear breakdown* Vacuolization*	Intercellular spaces Nucleus absent* Mitochondrial breakdown* Vacuolization*	Xylem proliferation Phloem proliferation Tracheary elements with non-uniformly thickened 2º walls Phloem distorting Xylem-phloem ratio ~1:1
Post-mature green seed (35 DAP)	Thick cell walls Absence of nucleus and most organelles* Vacuolization* Vacuole contents homogenous*	Intercellular spaces Vacuolization* Vacuole contents homogenous* Empty-walled cells or cell fragments*	Tracheary elements with non-uniformly thickened 2º walls Phloem vacuolating and crushing* Xylem-phloem ratio ~1:1

*Cellular features of programmed cell death.

DISCUSSION

By quantifying the overall growth of the funiculus and using microscopic techniques (light and TEM), I found that the funiculus increases in size and that large-scale histological changes as well as finer ultrastructural changes occur throughout development. This study provides the first histological description of funiculus development in the Brassicaceae and proposes functions conferred by the anatomical features observed. The initial rate of growth in the funiculus is rapid and dramatic before tapering off toward the end of seed development (Figure 2.1F, G). As the sole connecting structure between the seed and the parent plant, it is unsurprising that the funiculus expands to support the developing seed, especially during embryogenesis (Holdsworth et al. 2008). The structural organization of the funiculus is relatively simple and contains all three plant tissue systems: the epidermis (dermal tissue), cortex (ground tissue), and vascular strand (vascular tissue) (Figure 2.2). The developmental progression of each tissue system (summarized in Table 2.1) is addressed in terms of both ultrastructural and broader morphological changes and how these modifications function to fulfill the demands of seed development.

In the early stages of development, the epidermis of the funiculus increases in size through cell division and enlargement (Figure 2.2A, C). At later stages, the epidermis still increases in size, but because of cell wall thickening on the periclinal walls; the outer wall becomes especially thick by the end of development (Figure 2.2E, F). Although young primary walls are thin and somewhat flexible yet still strong (Cosgrove 2005), thicker walls better delimit the size and shape of the cell. Because the cell wall often represents the first impediment to herbivory attempts (Lucas et al. 2000) or pathogen invasion (Lagaert et al. 2009), additional wall material

in the epidermis could help the organ resist penetration to the vascular sap. Therefore, the

reinforced epidermal layer likely serves 2 functions: acting as a protective barrier (much like the

seed coat does for the embryo) to prevent access to the nutrient-rich cells of the vasculature, and

as a mechanism of structural support through primary cell wall thickening.

Over developmental time, cells of the epidermis become vacuolated, which is reminiscent of

processes associated with reduced cell activity. It is evident that cells of the epidermis are

degenerating in a pattern similar to that of PCD. PCD is a genetically orchestrated process of

deliberate cell destruction (Vianello et al. 2007) and can occur during the natural course of

development, as a response to abiotic stress, or as a hypersensitive response to inhibit pathogen

invasion (van Doorn et al. 2011). Although terminal dUTP nick and labeling (TUNEL) assays

are a common tool for confirming the nuclear fragmentation characteristic of PCD (Ning et al.

2002), I elected to use TEM to show the cellular process of PCD over developmental time

because it allows for a more detailed visualization of cell structures.

The PCD pattern observed in the epidermal and cortical layers of the canola funiculus most

closely conforms to vacuolar cell death as described by van Doorn et al. (2011). The authors

identify several general steps in this type of PCD: i) packaging of the cytoplasm by vesicles,

which then fuse with the lytic vacuole leading to a reduction in cytoplasmic volume that is

directly correlated to an increase in vacuolar volume; ii) intact organelles until the late stages of

PCD; and iii) rupture of the tonoplast and entire cellular clearance, which may or may not also

include the cell wall. Other features of developmental PCD are the degradation of plastids and

nuclei, cytoplasmic inclusions appearing in the vacuoles, and the ultimate breakdown of

mitochondria (Gaffal et al. 2007; van Doorn and Woltering 2005). All of these features occur in

both the epidermis (Figure 2.3) and the cortex (Figure 2.4) of the funiculus, and this kind of

intensive intracellular remodeling associated with autophagy is implicated in seed development

(Li and Vierstra 2012).

The major differences between the PCD observed in the epidermis compared to that observed

in the cortex are the rate at which the cell death progresses and the extent to which it occurs by

the end of development (Figures 2.3, 2.4; Table 2.1). The epidermal cells all undergo PCD at the

same rate, whereas the progress of PCD is variable among different parts of the cortex (Figure

2.4D, E). The outermost cortical cells degenerate first and more completely, resulting in the

collapse of the entire cell. The innermost cells undergo PCD at a delayed rate and become

entirely vacuolated, but still retain their cell walls (Figure 2.2C-E).

Generally, the ground tissue of the funiculus can be described as deteriorating over the

course of seed development as the rest of the funiculus expands, resulting in the formation of

large intercellular spaces (Figure 2.2). Therefore, the cortex in the later stages of funiculus

development can be described as aerenchymatous. Because this aerenchyma is formed through

the separation of cells from one another, its pattern of development is schizogenous (Drew et al.

2000). Aerenchyma formation serves two notable functions: reducing the amount of tissue that

needs to be aerated, and creating a route for oxygen circulation (Drew et al. 2000). This would be

critical for the funiculus, which spends its entire lifecycle enclosed in a fruit. As it grows larger,

the funiculus likely requires more extensive intercellular spaces to allow for gas transfer, likely

to support the developing seed and explaining why aerenchyma is not present in the much

smaller ovule.

Approximately 20-30% of light is capable of penetrating the silique wall enclosing the seeds

(Bennett et al. 2011). Yu et al. (2010) note that canola seeds are green and possess functional

chloroplasts throughout most of their development and Eastmond et al. (1996) report that

photosynthesis occurs in canola but is accomplished primarily via the embryo. Canola funiculi

are green in the mature ovule and remain green until at least the heart stage of seed development

(Figure 2.1A-C). Chloroplasts exist in the epidermis and cortex in the early stages of

development but begin to deteriorate toward the end of morphogenesis (Figures 2.3, 2.4).

Chloroplast degradation is, unsurprisingly, closely correlated to a decline in photosynthetic

capacity (Ghosh et al. 2001). The appearance and accumulation of plastoglobuli and the loss of

granal stacks and eventually thylakoid membranes characterize chloroplast senescence (Ghosh et

al. 2001). These features are consistent with the changes that occur in chloroplast ultrastructure

of the epidermal (Figure 2.3B, H) and cortical (Figure 2.4B, D, G) cells as the funiculus matures.

This suggests that the funiculus is photosynthetic until the embryo enlarges and achieves greater

autotrophic self-sufficiency.

From the ovule to the globular stage of seed development, the vascular strand, particularly

the phloem, becomes much larger (Figure 2.2A, B). Increasing the number of cells of the

vasculature, especially the phloem, may be in preparation for metabolically demanding stages of

seed development, such as the heart stage when new membranes and cell wall material is

deposited as part of the establishment of new tissue systems. Because nutritive compounds

accumulate in the embryo during seed maturation (Harada et al. 2010), the phloem is necessary

to conduct these products to the seed. Indeed, there is an increase in conducting cell types found

in the phloem as the funiculus develops through the morphogenesis phase (Figure 2.5C), with

these cells likely differentiating from the abundant parenchyma in the phloem region.

The vascular strand appears to function in transporting nutrients from adjacent tissues to the

seed; as it increases in size, there is a gradual depletion of nutrients from the cortex and

epidermis. However, given the data, it is difficult to determine the rate of nutrient flow through the funiculus and the percentage of nutrients being translocated from the maternal plant.

By the end of seed development, the phloem is crushed (Figure 2.5D, E). Because the cessation of seed metabolism (and the need for compounds to be transported into the seed) precedes dormancy (Graeber et al. 2012), maintaining the phloem would not be necessary. Gaffal et al. (2007) found that once the floral nectaries of *Digitalis purpurea* are no longer secretory, the phloem cells are disassembled through PCD. A similar process seems to occur in the phloem of the funiculus: the cells are much more vacuolated during the maturation phase and by the post-mature green stage, there are numerous vacuolar inclusions but no evidence of tonoplast membranes (Figure 2.5E) suggesting rapid deterioration of phloem integrity.

A profound increase in the number of cells of the xylem is notable in the maturation phase of development (Figure 2.2E, F) when cells of the embryo expand rather than divide. The increased water supply because of the addition of tracheary elements would allow for embryo elongation to transition from morphogenesis to maturation. TBO staining reveals the presence of lignified secondary cell walls in the tracheary elements of the xylem (Figure 2.2). The tracheary elements are also quite small, conferring a greater cell wall to lumen volume ratio that, along with the rigid secondary cell walls, would allow these cells to impart structural support for the organ in addition to functioning in transport. Because extensive xylem development also appears around the time that the epidermis of the funiculus thickens, this pattern suggests that the proliferation of tracheary elements in conjunction with the thickened epidermis may serve a mechanical support function for the enlarging seed (Figure 2.2), especially given the reduction in the ground tissue layer.

My results clearly illustrate that funiculus development is a dynamic process associated with

seed development and that changes in cellular organization are accompanied by changes in ultrastructure in the three tissue systems of the funiculus. These anatomical modifications that occur over developmental time correspond to major stages of seed development and serve to support the seed as it develops. Changes in the structural organization of the funiculus are likely necessary for normal seed growth. Understanding all of the genes responsible for programming these features will likely lead to improved seed performance in the future and are currently being investigated.

INTRODUCTION

Biological processes required to program plant development are controlled by large suites of genes that can be separated in both space and time. I have shown that dynamic cellular changes occur in the three tissue systems of the canola funiculus throughout seed development (Chapter 2). These changes include: cell proliferation, growth of the primary cell wall, and programmed cell death (PCD) in the epidermis; initial growth in the cortex, followed by PCD and transition to aerenchyma tissue; and tissue growth in both xylem and phloem of the vasculature. Although all the tissue systems undergo dramatic changes throughout the funicular lifecycle, the regulatory programming of this structure remains unresolved. Thus, understanding the networks underlying funiculus development should yield valuable information that can contribute to the directed manipulation of seed traits of agronomic importance.

The propose of this study is to investigate the genes responsible for funiculus development. I chose to focus my efforts on the globular seed because of the biological importance of this stage. In Brassicaceae seeds, the globular embryo is forming major primary tissues and is metabolically active (Harada et al. 2010). Belmonte et al. (2013) found that many sub-region-specific genes in the Arabidopsis seed become active at early developmental stages. My light micrographs reveal that all three tissue systems of the funiculus have changed by the globular stage as compared to the ovule stage (Figure 2.2A, B), suggesting that developmental changes are indeed occurring.

To investigate the three tissue systems of the funiculus and to better understand the developmental programs responsible for tissue system development, I used a combination of laser microdissection (LMD) coupled to next-generation RNA sequencing (RNA-seq) techniques. Because of the microscopic size of the target area of interest, the acquisition of the

individual tissue systems of the funiculus for profiling experiments would not otherwise by possible without the use of LMD. LMD is a technology that allows for the selection of tissues and individual cells from a heterogeneous sample without contamination from neighboring tissues and without direct contact by the user (Becker et al. 2014; Khan et al. 2014). Unlike other methods that rely on fluorescent (Zhang et al. 2008) or antibody (Tangrea et al. 2004) additional markers to aid in recognition of specific cell types, identifying the regions of interest for LMD is done through basic histological examination (Nelson et al. 2006). The tissues isolated and captured using LMD can then be subjected to downstream molecular approaches such as RNA-seq, which can provide useful data for the identification of differentially expressed genes (Becker et al. 2014).

RNA-seq data from individual tissue types would provide a high-resolution spatial account of differential transcript accumulation within the funiculus, a critical and understudied compartment of the seed. This current study expands on work previously reported by Belmonte et al. (2013) who profiled gene expression in every cell and tissue of the Arabidopsis seed over the course of development. The authors found that the genes involved in seed development represents 60% of the total number of genes in the Arabidopsis genome. These genes are spatially influenced, and networks of genes function together to regulate seed development. Gene ontology (GO) term enrichment of these extensive gene sets can accurately predict the functions of each region and sub-region of the Arabidopsis seed (Belmonte et al. 2013). Although this paper presents the most comprehensive transcriptome dataset of any seed to date, funiculus development was not explored, and no other literature exists that characterizes funiculus development from a molecular perspective.

To fully understand all of the genes required to program funicular development, next-generation sequencing must be utilized to profile global patterns of mRNA accumulation to study the transcriptome. Although many platforms for the detection and quantification of RNA exists, the introduction of next-generation sequencing technologies has profoundly increased throughput at progressively reduced costs (Wang et al. 2009). RNA-seq offers several advantages over previous methods of transcriptome analysis: i) little starting material is required for sequencing; ii) extreme accuracy in the quantification of transcript accumulation; iii) *a priori* knowledge of transcript sequences is not required; and iv) the generation of vast amounts of transcript sequence data (Becker et al. 2014).

Because several gigabytes of sequence data can be produced using RNA-seq, appropriate bioinformatics pipelines must be implemented to manage and process these data. Recently, bioinformatics has emerged as a multidisciplinary field that employs extensive mathematical, statistical and computational tools to process and analyze large-scale biological datasets such as those generated by sequencing (Pop and Salzberg 2008). Using bioinformatics tools to analyze RNA-seq data can yield unprecedented insight into gene activity. Differential gene expression (McGettigan 2013), transcripts with low abundance (Wang et al. 2009), novel transcripts (Roberts et al. 2011), and even alternative gene isoforms and transcript splice variants (Anders et al. 2012) can be elucidated.

The *Brassica napus* genome consists of 1130 millions of base pairs, represented by approximately 101,040 gene models (Chalhoub et al. 2014). Chalhoub et al. (2014) found that 96% of the genes are expressed between leaves and roots. Although this is one of the first detailed studies profiling the RNAs of canola, no data is currently available on reproductive structures and certainly none exists for the funiculus. In this chapter, I describe transcript

accumulation in the tissues of the funiculus and reveal putative developmental programs and

processes underlying the epidermis, cortex and vasculature. My results show that spatial patterns

of transcript accumulation are specific to each tissue type. For example, the epidermis appears to

function in cell wall growth and developmental programmed cell death (PCD); the cortex

functions in photosynthetic activity, possibly to produce nutrients that can be translocated into

other developing seed regions; and the vasculature functions in tissue proliferation and transport.

I further discuss how these biological processes play a role in seed development.

MATERIALS AND METHODS

1. LASER MICRODISSECTION (LMD)

1.1. Tissue processing

All solutions and tools used were RNase-free. Unless otherwise specified, tissue processing was completed in a rotary mixer at room temperature.

1.1.1. Fixation

Canola siliques 7 DAP were collected and cut transversely into smaller fragments, and placed in a vial of fixative of 25% glacial acetic acid and 63.75% ethanol. Fixation occurred undisturbed overnight at 4ºC.

1.1.2. Dehydration

The fixative was removed and replaced with 3x washes of 70% ethanol. After the final rinse, dehydration proceeded with a graded ethanol series: 85%, 95%, 100% (x2), with the tissues remaining in each solution for 30 minutes. Tissues were then further dehydrated with xylenes, which also served as the transition solvent. Tissues were placed in series of graded xylenes-ethanol solutions in the following ratios (*v/v*): 1:3, 1:1, 3:1, with the tissues remaining in each solution for 1 hour. The tissues were then placed in 100% xylenes overnight.

1.1.3. Transition infiltration

The next day, the previous xylenes solution was replaced with fresh 100% xylenes for 2 hours. After 2 hours, 6 Paraplast Plus paraffin chips (McCormick Scientific, St. Louis, MO, USA) were added to the vial. At the end of the day, another 10 chips were added and the vial left overnight.

1.1.4. Infiltration

The vial with the tissues was incubated at 42ºC for approximately 1.5 hours and then at 60ºC

for approximately 30 minutes. The xylenes/paraffin mixture was discarded and replaced with

100% pre-melted paraffin at 60ºC and the tissues incubated in a 60ºC oven. At the end of the

day, another paraffin change was performed and the tissues returned to 60ºC overnight.

1.2. Embedding

Another paraffin change was completed the next day and the tissues left to incubate at 60ºC.

Plastic weigh boats were filled with melted paraffin wax and the tissues emptied into the boats in

the afternoon. Using forceps, the tissues were quickly arranged into clusters and the weigh boat

left to cool at room temperature so that the paraffin could solidify. Cooled boats were stored at

4ºC overnight.

1.3. Blocking

Plastic tissue embedding rings (Fisher Scientific, Ottawa, ON, Canada) were filled with

melted paraffin wax and left to solidify at room temperature. Areas containing the clusters of

tissue were cut from the wax mould from the weigh boat. The areas were trimmed into squares

no larger than 1 inch^2 and attached to the pre-filled, solid embedding rings using melted paraffin.

The embedding rings with the blocks of tissues attached were stored at 4ºC overnight.

1.4. Sectioning, mounting and de-paraffinization

Prior to sectioning, each block was trimmed into a bilateral trapezoid shape in such a way as

to minimize surrounding wax and maximize the area of tissue in the block face. Blocks were cut

into 10 µm thick sections using disposable steel blades on a Leica RM2245 microtome (Leica

Microsystems, Wetzlar, Germany). Ribbons containing many funiculi were mounted on

MembraneSlides (Leica Microsystems, Wetzlar, Germany), glass slides with a polyethylene

naphthalate (PEN) membrane film on the surface, using autoclaved, DepC-treated water as the

mounting medium. Excess water was drained off, and the slides were dried on a slide warmer set to approximately 33ºC.

Completely dry slides were de-paraffinized through submergence in a first bath of xylenes and then immediately transferred to a second, fresh xylenes solution. The entire process, including transfer time, was completed in 1 minute. De-paraffinized slides were stored in a slide box at room temperature.

1.5. Laser capture of tissues

LMD was carried out using the Carl Zeiss PALM MicroBeam system (Carl Zeiss, Oberkochen, Germany). The desired tissue fragment was traced using the Freehand Tool in the PALMRobo software version 4.3. This created an "element" that the laser would then carve out and catapult, along with the underlying film, against gravity into a collection tube. The values for the laser speed and energy of the beam were specified in such a way as to minimize the amount of energy necessary. These values were approximately 15 for speed and approximately 45 for energy.

Epidermis, cortical and vascular tissue (Figure 3.1) were collected individually in separate 0.5 mL microcentrifuge tube caps (Fisher Scientific, Ottawa, ON, Canada) lined with 30 µL of lysis buffer (from the Ambion® RNAqueous®- Micro Kit [Life Technologies, Carlsbad, CA, USA]). Whole funiculi were also collected as a control. The collection period for a single cap did not exceed 1.5 hours. If the lysis buffer did evaporate during this time, 20-30 µL of lysis buffer was added back to the cap and the added volume noted.

Samples that were not used immediately for RNA extractions were stored at -80ºC.

2. ISOLATION OF RNA FROM LASER MICRODISSECTED SAMPLES

2.1. RNA extraction

At least 20 elements from funiculi from at least 3 different plants were combined to comprise a single bioreplicate. Three bioreplicates per tissue type as well as the three bioreplicates of whole funiculi were processed.

RNA was extracted using the Ambion® RNAqueous®- Micro Kit (Life Technologies, Carlsbad, CA, USA). Samples that were not analyzed immediately were stored at -80ºC.

2.2. Assessing RNA quality of LMD-collected samples using the Agilent 2100 Bioanalyzer

The extracted RNA samples were loaded into Agilent RNA 6000 Pico Chips (Agilent Technologies, Santa Clara, CA, USA) and run in an Agilent 2100 Bioanalyzer (Agilent Technologies, Santa Clara, CA, USA) according to manufacturer's instructions with two notable modifications: replacement syringes were not used, and the RNA sample tubes were tapped, not vortexed, to mix before loading the sample into the chip.

The kit analyzes total RNA of a given sample by using gel electrophoresis to separate nucleic acid fragment, and produces a digital electropherogram. The Bioanalyzer 2100 Expert Software (Agilent Technologies, Santa Clara, CA, USA) also calculates an RNA integrity number (RIN) from the electropherogram tracing which is a reliable indicator of RNA quality (Schroeder et al. 2006). The RIN ranges from 1-10, with 1 indicating that the sample is completely degraded and 10 representing a sample with completely intact RNA (Schroeder et al. 2006).

3. NEXT-GENERATION RNA SEQUENCING

3.1. Constructing cDNA libraries for RNA-seq

3.1.1. cDNA synthesis and amplification

cDNA was constructed from the RNA sample using the Ovation® RNA-Seq System V2 (NuGEN, San Carlos, CA, USA) according to manufacturer's instructions. This kit is able to amplify low quantities of RNA and is successful in amplifying partially degraded RNA samples (Tariq et al. 2011).

Eukaryotic RNA amplification for RNA-seq tends to suffer from contamination from structural RNAs such as rRNA and tRNA (Tariq et al. 2011). The Ovation® kit utilizes Ribo-SPIA (single primer isothermal amplification) technology to amplify the RNA from multiple sites along the strand independent of the abundance of 3' end RNA fragments (Kurn et al. 2005), and then amplifies the cDNA using the SPIA® system developed by NuGEN. This has two benefits: i) avoiding 3' end-biased amplification and amplification based on the presence of poly-A tails (not all transcripts encode poly-A tails) that other amplification methods tend to use; and ii) allows for the use of partially degraded RNA as an acceptable starting material.

3.1.2. Preparing the cDNA library for sequencing

The library was fragmented into a target size range by using the NEBNext® dsDNA Fragmentase® kit (New England Biolabs, Ipswich, United Kingdom). The library was further modified using the Illumina TruSeq™ RNA Sample Preparation v2 kit (Illumina, San Diego, CA, USA) using the low-throughput protocol according to manufacturer's instructions. This process involved: i) modifying the fragment ends so that they would not ligate to one another, and adding an additional adenosine base to the fragments to facilitate adapter (which have a complementary tyrosine base) ligation; ii) ligation of fragments to unique adapters (multiplexing) to allow for pooling of the samples so that multiple samples could be run in a single lane of a flow cell to maximize resource efficiency; iii) purification of the products to remove the adapters that failed to ligate and/or adapters that have dimerized, and insert read

lengths that are unsuitable for sequencing; and finally, iv) PCR amplification to enrich the fragments via the use of primers that bind to the adapters.

3.1.3. Validating the library using the Agilent 2100 Bioanalyzer

To ensure that fragment sizes fell within the suitable range and had an appropriate size distribution, a sample of each library was loaded into Agilent High Sensitivity DNA Chips (Agilent Technologies, Santa Clara, CA, USA) and run on the Agilent 2100 Bioanalyzer (Agilent Technologies, Santa Clara, CA, USA) according to manufacturer's instructions. This quality verification is an important step as unrefined libraries may suffer from contaminants such as remaining adapters or smaller fragments of the cDNA, which can reduce the productivity of the sequencing (Quail et al. 2012).

Quail et al. (2012), in evaluating different methods of library preparation and library quality verification prior to sequencing, found that a well-prepared library had an average fragment size of 300-500 bps. With the exception of the Cortex 3 sample, the prepared libraries fell within this range (Tables 3.1-3.4). Because the library for Cortex 3 was not suitable for sequencing (Table 3.2), it was excluded from the pool.

3.2. RNA-seq

The Illumina HiSeq 2500 platform was used to sequence the multiplexed sample on a single lane of a flow cell according to manufacturer's instructions. This was completed at the University of California, Davis Genome Center. Each samples was sequenced at 50 bp, single end reads.

4. ANALYSIS OF THE SEQUENCING DATA USING BIOINFORMATICS AND VISUALIZATION TOOLS

Because the analysis of the sequencing data required the generation of additional large-scale

datasets, supplementary materials can be found in digital format on the University of Manitoba's

MSpace database.

4.1. Analyzing the sequencing data using the Tuxedo pipeline

Processing of the sequencing data was completed using the Tuxedo suite of tools

(Bowtie/TopHat/Cufflinks; Givan et al. 2012) available through Galaxy (https://usegalaxy.org/),

an open access web source for academics that streamlines multiple bioinformatics software

programs into a user-friendly, somewhat customizable workflow. The default settings pre-set by

Galaxy were applied in each step of the Tuxedo workflow.

4.1.1. Grooming the FASTQ sequence files

The sequencing data was packaged as a compressed FASTQ file. Uncompressing this file so

that it was suitable for further analyses by the bioinformatics software is referred to as

"grooming" the data. This was done using the FASTQ Groomer tool in Galaxy.

4.1.2. Aligning the reads to the *B. napus* reference genome

Because the sequence lengths of the reads are so short (50 bps long), they must first be

mapped (aligned) to a reference. Even with transcript sequences, the standard approach is to map

the reads to a reference genome (instead of a reference transcriptome) and then compare the

aligned reads to known annotated transcripts (Ramsköld et al. 2012). Alignment was completed

using the software program TopHat (which implements the program Bowtie [another alignment

tool; Trapnell et al. 2011]) version 2.0.9 and a FASTA format of a draft genome of *Brassica*

napus (genotype DH12075) that was made available to me through the Canadian Canola

Sequencing Initiative (Can-Seq) consortium.

4.1.3. Transcript assembly and measure of relative abundance

A BAM file is outputted from each of the alignments with TopHat. This file contains the accepted hits of the reads to a mapped location – i.e. the successfully aligned reads. Using the BAM files from TopHat, the program Cufflinks version 2.1.1 was used to assemble and estimate the abundances of the transcripts. The output from this software are FPKM (fragments per kilobase of exon per million mapped reads) values, which is a normalized measure of the number of reads per transcript (i.e. the number of times to which a transcript is mapped); It is an indicator of transcript abundance (Trapnell et al. 2012).

4.2. Visualization of the sequencing data

4.2.1. Quality assessment and determination of the relationships between bioreplicates

To determine the relationships between bioreplicates and tissue types, two Bioconductor version 2.14 software packages were used to visualize the data: sRAP (simplified RNA-seq analysis pipeline) version 1.4.1 and DESeq (differential expression of RNA-seq data at the gene level) version 1.16.0. Only those transcripts that were considered to be detected (FPKM $\geq$ 1) in at least one sample were included in the analysis. Both of these programs require raw counts (RCs; as opposed to an FPKM values) as the input values, so RCs were calculated as follows:

RC = FPKM × length of transcript (in kilo-base pairs) × # of mapped reads (in millions)

FPKM and transcript length values were both found in the transcript expression file outputted from Cufflinks, and the number of mapped reads could be found in the alignment summary file outputted from TopHat.

Because initial runs of the programs consistently showed that the Whole funiculus 2 (WF2) bioreplicate grouped separately from all other samples, all grouping and remaining analyses were completed without including the WF2 data.

4.2.2. Quantifying the unique transcripts found in individual tissue layers

Using VENNY (http://bioinfogp.cnb.csic.es/tools/venny/index.html), an online tool

developed by Oliveros (2007) that compares lists, I was able to quantify the number of

transcripts found in all tissue layers of the funiculus (all bioreplicates of epidermis, cortex, and

vasculature) vs. the number of transcripts found in the whole funiculus bioreplicates. Only

detected transcripts (as defined as any transcript with an FPKM ≥ 1 in at least one of the

samples) were included in the analysis.

Of the transcripts uniquely detected in individual tissue systems, a tissue specificity index (*I*)

was calculated according to the following formula modified from Tong et al. (2013) and Yanai et

al. (2005):

$$I_g = \sum_{t=1}^{n} \left(\frac{1 - \left(FPKM_{g,t}/FPKM_{g,max}\right)}{n - 1} \right)$$

In this formula, n = the number of samples (tissues/tissue bioreplicates); $FPKM_{g,t}$ = the

FPKM value of the gene (g) in the tissue/tissue bioreplicate (t); and $FPKM_{g,max}$ = the highest

FPKM value of that gene (g) across all samples. The numerical output of this calculation is a

value $0 \leq I_g \leq 1$, with 0 meaning that the transcript is globally detected (i.e. not tissue-specific)

and 1 meaning that the transcript was detected in only one of the samples surveyed (i.e. very

tissue-specific). A Wilcoxon rank-sum test (conducted via the statistical software program JMP

version 10.0.1) was used to determine the statistical significance of *I* between the two groups of

transcripts.

The distribution of transcript abundance (low transcript abundance: $1 \leq FPKM < 5$; moderate

transcript abundance: $5 \leq FKPM < 25$; high transcript abundance: $25 \leq FPKM$) in each

bioreplicate of each tissue was also calculated and reported.

4.2.3. Identification of dominant patterns of transcript accumulation

Dominant patterns (DPs) of transcript accumulation were identified using fuzzy *K*-means

(FKM) implementation FANNY in R (http://cran.r-project.org/web/packages/cluster/cluster.pdf). FKM analysis clusters data points (i.e. genes) based on similarity but allows a single data point to belong to more than one cluster (i.e. DP). The advantage of a fuzzy method of clustering (instead of hard clustering in which the clusters are completely discrete and a data point may only be assigned to one cluster), is that it more accurately reflects the fact that genes can be responsible for multiple biological functions, and can be regulated differently in different pathways and under different conditions (Tari et al. 2009).

For my analysis, I included the transcripts that were detected in at least one sample (FPKM $\geq$ 1) and calculated a mean FPKM value for that transcript in each tissue (i.e. the average FPKM between the bioreplicates of each tissue). I used a K choice of 10 (to instruct the program to define 10 centroid data points and therefore generate 10 clusters) and a Pearson's correlation coefficient of 0.8 (the minimum similarity value between data points for them to group together in a cluster). Each gene was assigned a cluster membership value (m), indicating how well it belonged to a particular pattern. The cutoff m value was 1.05.

4.2.4. Identification of enriched GO terms found in each tissue system of the funiculus

The genes belonging to each DP were matched to the corresponding AGI (Arabidopsis Genome Initiative) gene IDs using a reference annotation file. The lists of Arabidopsis genes were inputted into ChipEnrich version 1.42a software (http://seedgenenetwork.net/presentation#software), a program that can identify enriched gene ontology (GO) terms within large-scale gene sets (Khan et al. 2014). A GO term was considered enriched if the $\log_{10} p$ value $\leq$ -3 (i.e. $p \leq 0.001$).

A heatmap showing the enriched GO terms associated with select DPs was generated using the Conditional Formatting tool in Microsoft Excel version 14.0.7.

5. TRANSMISSION ELECTRON MICROSCOPY (TEM)

Tissue processing, embedding, blocking, sectioning, visualization and image modifications were performed exactly as previously described in Chapter 2.

RESULTS

1. ACQUISITION AND AMPLIFICATION OF RNA FROM LASER MICRODISSECTION-COLLECTED SAMPLES

To identify the three tissue systems of the canola funiculus (Figure 3.1A) for LMD, tissues were processed and embedded in paraffin wax. Figure 3.1B shows a paraffin-embedded globular stage funiculus as would be used for LMD. As compared to methacrylate-embedded tissues (e.g. Figure 2.2B), the image quality is noticeably different because of the different processing protocols used. The increased section thickness leads to reduced image resolution. The lack of a coverslip and lack of differential staining also contributes to the difficulty in clear tissue delineation, especially between the ground tissue and the vasculature. The epidermis and peripheral cortex layers, however, can be clearly distinguished, and where the boundaries between tissues were difficult to define with certainty (e.g. between the vascular strand and the innermost cortical cells), care was taken to avoid collecting those areas to prevent sample contamination.

For epidermis, cortex and vascular tissue, respectively, approximately 2 million μm^2, approximately 3 million μm^2, and approximately 1.5 million μm^2 of LMD-excised tissue was necessary to constitute a single bioreplicate with an RNA yield > 10 ng (Tables 3.1-3.3). However, LMD-collected samples yielded RNA that was partially degraded, with RIN values no greater than 6.5. Although the two ribosomal peaks (18S and 28S) are noticeable in the electropherograms as would be expected for eukaryotic RNA, there is a shift toward the left of the first peak (18S subunit), indicating RNA breakdown. RNA degradation was the least severe in whole funiculi cut using LMD as opposed to the isolated tissues of the funiculus, which exhibited more degraded RNA (Tables 3.1-3.4).
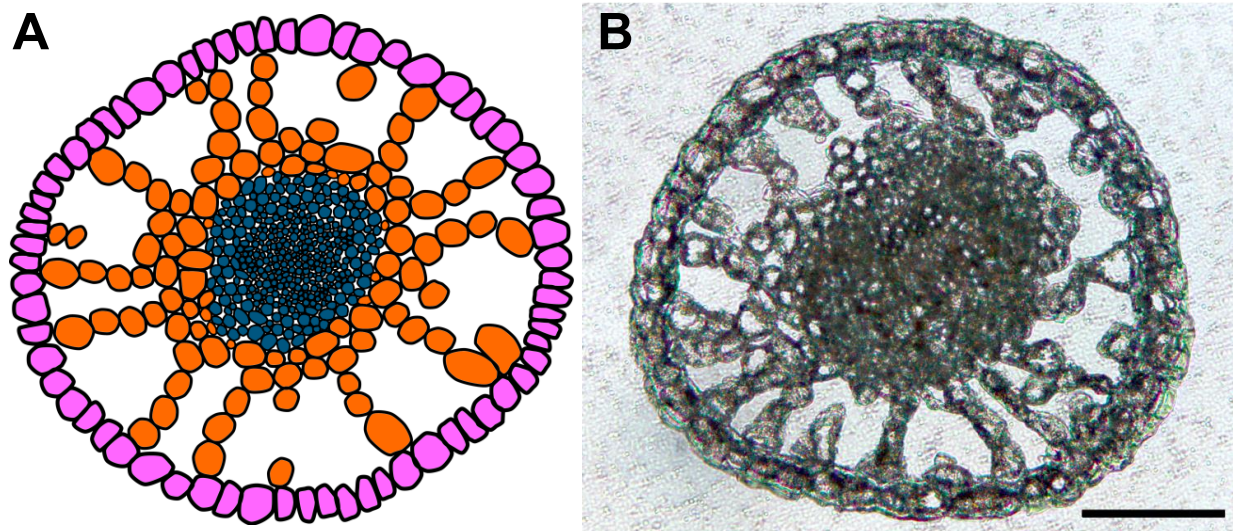
Figure 3.1: Representative cross-sections of a canola (*Brassica napus*) funiculus 7 days after pollination (globular stage seed) as would be used for laser microdissection.
A: Schematic diagram of the funiculus showing the three plant tissue systems. Pink = epidermis; Orange = cortex; Navy = vasculature.
B: 10 μm thick paraffin-embedded section of the funiculus. Scale bar = 100 μm.

Table 3.1: Data output including RNA quality, RNA and cDNA quality and quantity, and electropherogram tracings from the Agilent 2100 Bioanalyzer of LMD-collected canola (*Brassica napus*) funiculus epidermis.
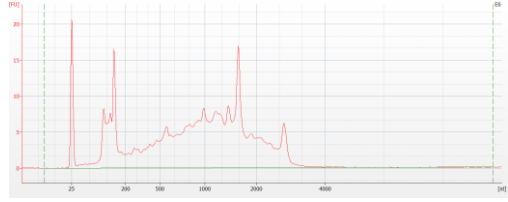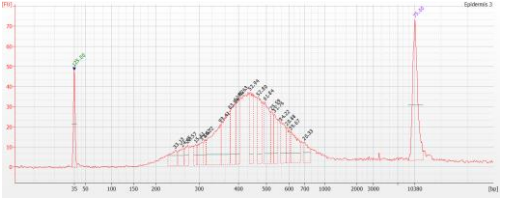
Tissue			Electropherogram tracings from the Agilent 2100 Bioanalyzer	
			Isolated RNA	cDNA library
Epidermis 1	Surface area excised (μm^2)	1 861 405		
	RIN	4.7		
	[RNA] (pg/μL)	742		
	RNA yield (ng)	11.1		
	cDNA yield (μg)	2.3		
Epidermis 2	Surface area excised (μm^2)	1 683 227		
	RIN	5.1		
	[RNA] (pg/μL)	678		
	RNA yield (ng)	10.8		
	cDNA yield (μg)	2.8		
Epidermis 3	Surface area excised (μm^2)	2 034 986		
	RIN	4.5		
	[RNA] (pg/μL)	1121		
	RNA yield (ng)	17.9		
	cDNA yield (μg)	3.4		
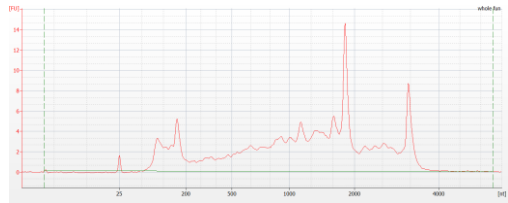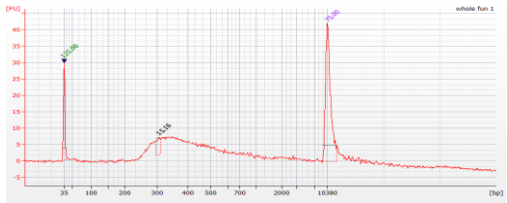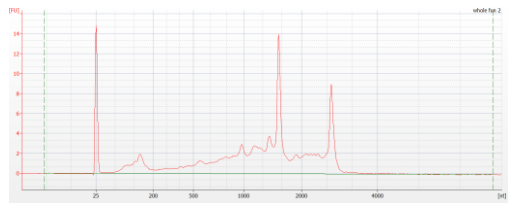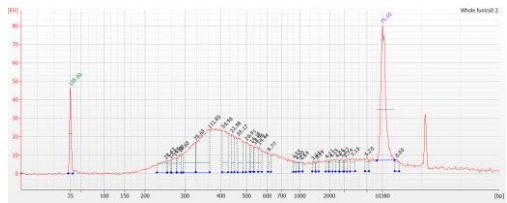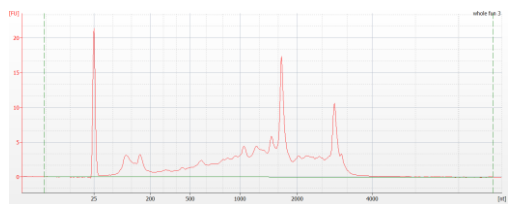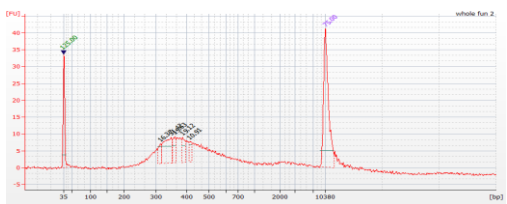
Table 3.2: Data output including RNA quality, RNA and cDNA quality and quantity, and electropherogram tracings from the Agilent 2100 Bioanalyzer of LMD-collected canola (*Brassica napus*) funiculus cortex.

Tissue			Electropherogram tracings from the Agilent 2100 Bioanalyzer	
			Isolated RNA	**cDNA library**
Cortex 1	Surface area excised (μm^2)	3 457 914		
	RIN	5.1		
	[RNA] (pg/μL)	926		
	RNA yield (ng)	13.9		
	cDNA yield (μg)	2.7		
Cortex 2	Surface area excised (μm^2)	3 577 213		
	RIN	4.6		
	[RNA] (pg/μL)	888		
	RNA yield (ng)	14.2		
	cDNA yield (μg)	1.9		
Cortex 3	Surface area excised (μm^2)	4 138 996		
	RIN	4.5		
	[RNA] (pg/μL)	504		
	RNA yield (ng)	8.1		
	cDNA yield (μg)	1.5		

Test test

Table 3.4: Data output including RNA quality, RNA and cDNA quality and quantity, and electropherogram tracings from the Agilent 2100 Bioanalyzer of LMD-collected canola (*Brassica napus*) whole funiculus.
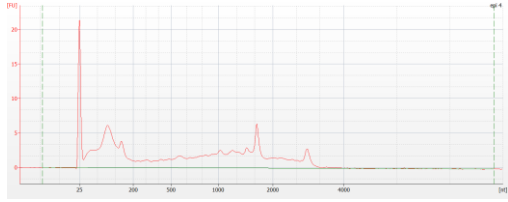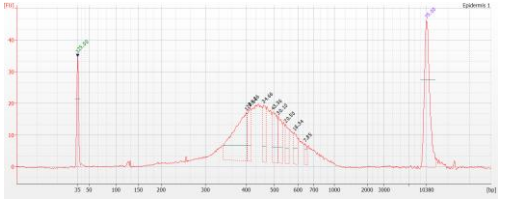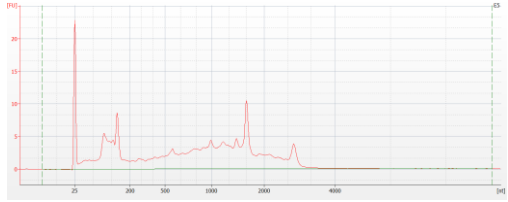
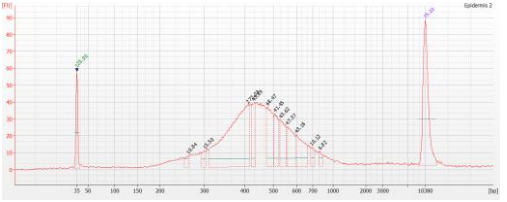| Tissue			Electropherogram tracings from the Agilent 2100 Bioanalyzer	
			Isolated RNA	cDNA library
Whole Funiculus 1	Surface area excised (μm^2)	7 849 408		
	RIN	5.1		
	[RNA] (pg/μL)	1305		
	RNA yield (ng)	19.6		
	cDNA yield (μg)	1.1		
Whole Funiculus 2	Surface area excised (μm^2)	3 812 119		
	RIN	6.5		
	[RNA] (pg/μL)	523		
	RNA yield (ng)	7.8		
	cDNA yield (μg)	2.7		
Whole Funiculus 3	Surface area excised (μm^2)	3 019 831		
	RIN	6.4		
	[RNA] (pg/μL)	885		
	RNA yield (ng)	13.3		
	cDNA yield (μg)	1.1		

Tables 3.1-3.4 shows the electropherograms of the amplified and prepared cDNA libraries from the isolated RNA samples. Almost all of the libraries exhibited a suitable fragment size distribution range anchored around a single peak size. However, the library for the Cortex 3 sample had a broader fragment size range, with two noticeable shoulders in the electropherogram tracing (Table 3.2). Although the right shoulder is within an appropriate fragment size range, the left shoulder of smaller fragments indicates the presence of contaminants, possibly from adapter dimers. Because the Cortex 3 sample did not have a well-prepared library, it was not multiplexed with the other samples.

2. RNA SEQUENCING DATA

2.1. Read counts and alignment to the B. napus genome

Approximately 10-25 million reads were generated per tissue sample, with 73.8-84.3% (average 81.5%) of those reads successfully aligning to the *B. napus* genome (Table 3.5). Of these aligned reads, an average of approximately 14% were uniquely mapping reads (Table 3.5). This indicates that although a small percentage of the total *B. napus* genome is represented by the funiculus, some transcripts are very abundant and are therefore highly represented by the number of reads that align to these transcripts. A modified summary of the alignment files outputted from Cufflinks, showing the gene ID, FPKM value and transcript length is available in Supplementary Dataset 1.

2.2. The relationship of funicular tissues to one another can be determined using various analytical methods

To determine the relationship between samples, I used DESeq to generate a principal component analysis (PCA), which shows that the bioreplicates of each tissue type cluster

Table 3.5: Alignment of RNA-seq reads to a *Brassica napus* draft genome using TopHat (version 2.0.9) and default settings* in Galaxy (https://usegalaxy.org/).

Tissue sample	Number of reads generated from sequencing	Aligned reads		Unique reads		
		Total number	Percentage	Total number	% of total reads	% of mapped reads
Epidermis 1	10,248,360	7,784,581	76.0	1,007,545	9.8	12.9
Epidermis 2	12,592,320	10,161,403	80.7	1,009,673	8.0	9.9
Epidermis 3	14,413,070	12,133,247	84.2	1,420,888	9.9	11.7
Cortex 1	15,167,122	12,620,380	83.2	1,141,584	7.5	9.0
Cortex 2	20,975,845	17,454,109	83.2	2,096,872	10.0	12.0
Vasculature 1	13,080,850	10,801,260	82.6	1,431,744	10.9	13. 3
Vasculature 2	15,064,817	12,492,706	82.9	1,410,314	9.4	11.3
Vasculature 3	18,829,388	15,486,902	82.2	2,093,581	11.1	13.5
Whole funiculus 1	24,769,916	20,653,924	83.4	2,063,101	8.3	10.0
Whole funiculus 2	17,789,844	13,132,864	73.8	4,740,018	26.6	36.1
Whole funiculus 3	23,562,229	19,866,331	84.3	2,534,396	10.8	12.8

* Default settings:

Max realign edit distance: 1000

Max edit distance: 2

Library type: FR unstranded

Final read mismatches: 2

Use bowtie –n mode: no

Anchor length: 8

Maximum number of mismatches that can appear in the anchor region of spliced alignment: 0

The minimum intron length: 70

The maximum intron length: 500,000

Allow indel search: yes

Max insertion length: 3

Max deletion length: 3

Maximum number of alignments to be allowed: 20

Minimum intron length that may be found during split segment (default) search: 50

Maximum intron length that may be found during split segment (default) search: 500,000

Number of mismatches allowed in each segment alignment for reads mapped independently: 2

Minimum length of read segments: 25

Use own junctions: no

Use coverage search: no

Use microexon search: no

Do fusion search: no

Use Bowtie2 settings: no

together (Figure 3.2A). The exception to this is the aberrant WF2 sample, which grouped

separately, not only from the other WF bioreplicates, but from all other tissues (Figure 3.2A).

Therefore, further analyses were completed excluding the WF2 data to prevent confounding

results.

Figure 3.2B shows a dendrogram illustrating the relationship between tissue types, and

reveals that the epidermis and cortex tissues are more similar to one another, and the vasculature

groups with the whole funiculus. This is in agreement with the PCA in Figure 3.2A.

2.3. Tissue-specific transcript detection uncovered by using LMD

RNA-seq of the funicular tissues revealed a total of 45,394 detected transcripts (FPKM ≥ 1;

Figure 3.3A). Sequencing of the whole funiculus only uncovered 34,917 transcripts, but when

the individual tissue samples collected using LMD were compared to the whole funiculus, I was

able to detect an additional 10,477 transcripts; This accounts for almost a quarter of all of the

transcripts identified. This demonstrates that using LMD to capture individual tissues of the

funiculus improves the number of transcripts detected at the RNA level compared to whole

funiculus samples.

A tissue specificity index (I) was calculated and assigned to each transcript. Figure 3.3B

shows that of the 10,477 tissue-specific transcripts uncovered using LMD, the median I value

(0.736) is greater compared to the median I value (0.554) of the entire detected transcript set.

According to a Wilcoxon rank-sum test, the difference in indices is significant ($p < 0.0001$). A

complete list of the tissue-specific as well as whole funiculus transcripts, and their associated I

values, is available in Supplementary Dataset 2.

2.4. Similar numbers of transcripts are found in all funiculus tissue samples
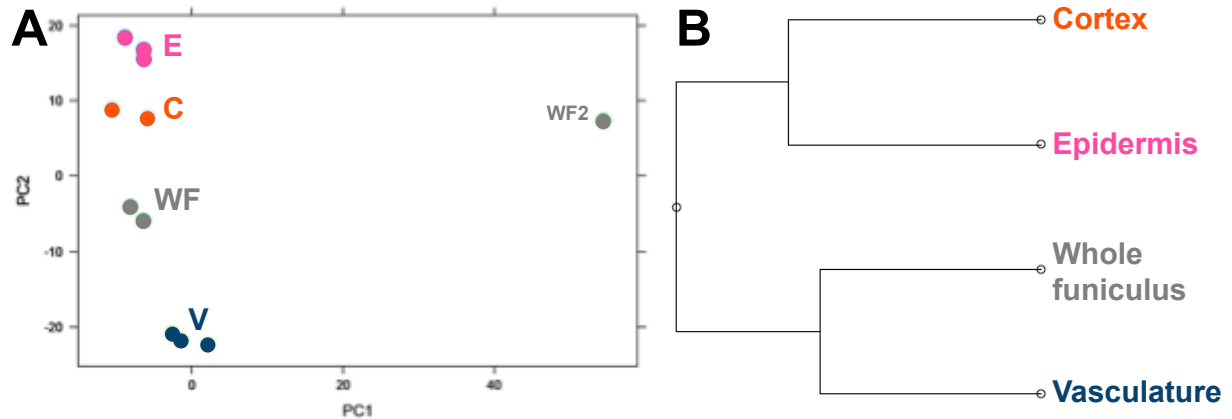
Figure 3.2: Grouping of RNA-seq data from the different tissues (epidermis, cortex, vasculature, whole funiculus) of the globular stage canola (*Brassica napus*) funiculus.
A: PCA generated using DESeq. Tissue bioreplicates group together and separately from other tissue types. WF2 is an exception and does not group with any of the other samples, therefore, it was excluded from further analyses. E = epidermis; C = cortex; V = vasculature; WF = whole funiculus.
B: Dendrogram generated using sRAP. The epidermis and cortex tissues are similar to one another, and different from the vasculature and whole funiculus, which are similar to each other. WF2 was not included in this analysis.
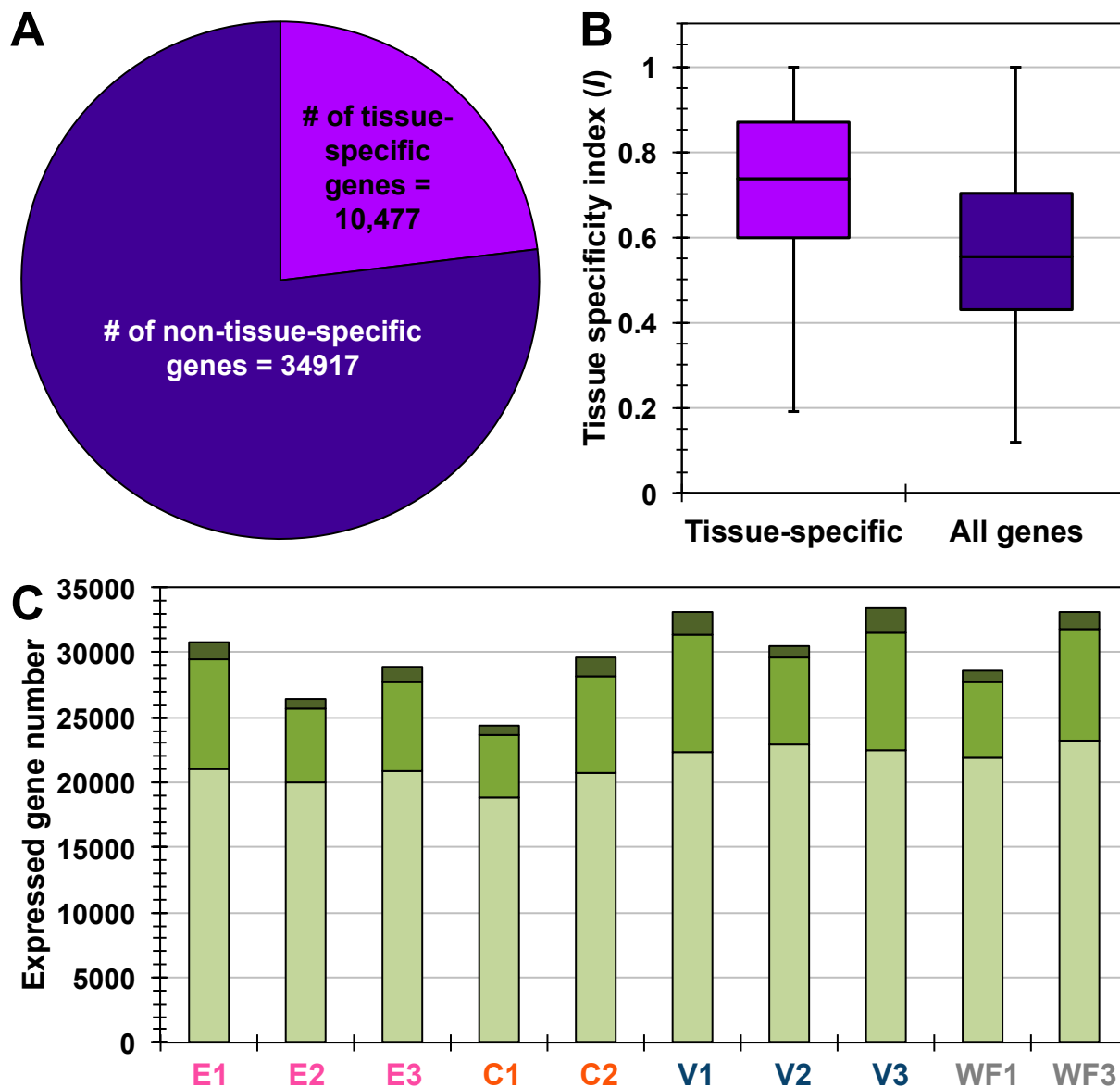
Figure 3.3: Quantification of transcript abundance in LMD-acquired tissues from the globular stage canola (*Brassica napus*) funiculus.

A: Pie chart showing the number of tissue-specific transcripts (transcripts detected only in the epidermis, cortex, and/or vasculature) vs. transcripts found in the whole funiculus (WF) organ.

B: The profile of the tissue specificity indices (*I*; as calculated in M+M) of tissue-specific transcripts (those found only in the epidermis, cortex, and/or vasculature) vs. all detected transcripts. Tissue-specific transcripts have a significantly higher *I* value than non-tissue-specific trancripts (Wilcoxon rank-sum test, $p < 0.0001$).

C: Distribution of the number of low abundance ($1 \leq FPKM < 5$; lighter green), moderate abundance ($5 \leq FPKM < 25$; green), and highly abundant ($25 \leq FPKM$; darker green) transcripts found in the epidermis (E), cortex (C), vasculature (V), and whole funiculus (WF) tissue bioreplicates.

A range of 24,337 to 33,463 transcripts were considered detected (FPKM ≥ 1) in all tissue

samples. I then divided the transcripts into those that showed low, moderate and high abundane.

Similar numbers of low abundance ($1 \leq$ FPKM < 5; approximately 67-77% of the total number

of detected transcripts), moderate abundance ($5 \leq$ FKPM < 25; approximately 20-27% of the

total number of detected transcripts), and highly abundant ($25 \leq$ FPKM; approximately 3-5.5%

of the total number of detected transcripts) transcripts were detected in all samples (Table 3.6,

Figure 3.3C). This suggests that although there are similar numbers of transcripts in the

individual tissues of the funiculus, the biological processes operative within these tissues are

likely different given the putative function of each tissue type as described in Chapter 2.

2.5. Fuzzy **K-***means clustering and GO enrichment analysis reveals tissue-specific patterns of transcript accumulation*

Using FKM analysis, 10 DPs of transcript accumulation were generated (Figure 3.4), with an

average of 2772 genes per DP, and a range of 753 (DP1) to 6329 (DP5) genes. A complete list of

the transcripts found in each DP, as well as their *Arabidopsis thaliana* homologue AGI ID, is

provided in Supplementary Dataset 3. Using the ChipEnrich program, I was able to identify

enriched GO terms associated with each pattern. The complete list of GO terms (with their $\log_{10}$

p values) associated with each pattern can found in Supplementary Dataset 4, and the list of

genes found in each GO term can be found in Supplementary Dataset 5.

The DPs generated by the FKM analysis show that mRNA accumulation tend to be tissue-

specific, as there is little similarity among the patterns (Figure 3.4), suggesting that unique

transcripts associated with a particular pattern can reveal what biological processes are occurring

in a particular tissue. DP3 shows transcripts that are highly abundant in the epidermis (Figure

Table 3.6: Distribution of transcript abundance among each tissue bioreplicate of the globular stage canola (*Brassica napus*) funiculus. Low transcript abundance: 1 ≤ FPKM < 5; Moderate transcript abundance: 5 ≤ FPKM < 25; High transcript abundance: 25 ≤ FPKM.

Tissue	Total # of detected transcripts	Low transcript abundance		Moderate transcript abundance		High transcript abundance	
		# of transcripts	% of total transcript accumulation	# of transcripts	% of total transcript accumulation	# of transcripts	% of total transcript accumulation
Epidermis 1	30,837	21,070	68.32	8,364	27.12	1,404	4.55
Epidermis 2	26,423	20,038	75.83	5,661	21.42	726	2.75
Epidermis 3	28,896	20,802	71.99	6,926	23.97	1,168	4.04
Cortex 1	24,337	18,834	77.39	4,735	19.46	768	3.16
Cortex 3	29,624	20,766	70.10	7,455	25.17	1,403	4.74
Vasculature 1	33,163	22,400	67.55	8,965	27.03	1,798	5.42
Vasculature 2	30,519	22,913	75.08	6,658	21.82	948	3.11
Vasculature 3	33,463	22,516	67.29	9,057	27.066	1,890	5.65
Whole funiculus 1	28,617	21,827	76.27	5,934	20.74	856	2.99
Whole funiculus 3	33,129	23,239	70.15	8,576	25.89	1,314	3.97
All LMD-acquired tissues	58661						
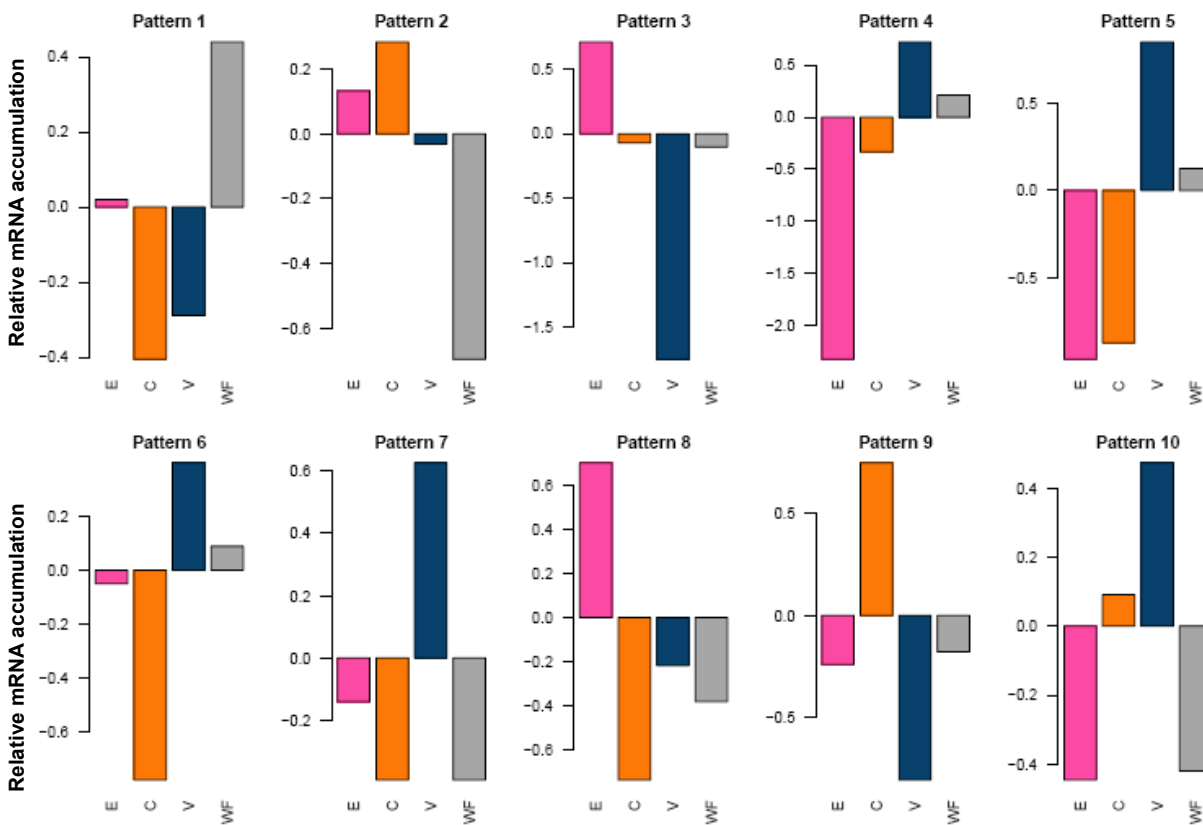
Figure 3.4: Dominant patterns of mRNA accumulation as identified by fuzzy *K*-means clustering of detected transcripts (FPKM ≤ 1) in the different tissue systems (epidermis – E, pink; cortex – C, orange; vasculature – V, navy) of the globular stage canola (*Brassica napus*) funiculus, as well as the whole funiculus (WF, grey).

3.5A, B). Many of the most highly enriched (i.e. lowest p value) GO terms were related to cell wall synthesis such as Golgi apparatus, cell wall, and carbohydrate biosynthetic process (Figure 3.5A). Plant-type cell wall, anchored to plasma membrane, cell surface, and cellulose synthase activity were all GO terms that were statistically enriched only in DP3. Some of the *Brassica napus* homologous genes found in these GO terms include: *TUBULIN ALPHA-6* (*TUA6*, AT4G14960), *CELLULOSE SYNTHASE 3* (*CESA3*, AT5G05170), *XYLOGLUCAN ENDOTRANSGLUCOSYLASE/HYDROLASE 17* (*XTH17*, AT1G65310), *GALACTURONOSYLTRANSFERASE 15* (*GAUT15*, AT3G58790), *GALACTURONOSYLTRANSFERASE-LIKE 3* (*GATL3*, AT1G13250), and *FASCICLIN-LIKE ARABINOGALACTAN PROTEIN 13* (*FLA13*, AT5G44130).

TEM images (Figure 2.3E, 3.5C) show numerous Golgi and their associated vesicles located proximal to the outer tangential cell wall of epidermal cells. This suggests that the function of the Golgi in the epidermis of globular stage funiculi is to deliver material to enlarge the cell walls over the course of development (Figure 2.3).

Other GO terms that are enriched in DP3 are related to response to abiotic stress and response to hormones (Figure 3.5A). These GO terms are: response to salt stress, response to jasmonic acid stimulus, response to abscisic acid stimulus, response to gibberillin stimulus, response to cold, response to ethylene stimulus, and response to water deprivation. Examples of the genes found in these GO terms are: *WRKY DNA-BINDING PROTEIN 25* (*WRKY25*, AT2G30250), *ETHYLENE RESPONSIVE ELEMENT BINDING FACTOR 4* (*ERF4*, AT3G15210), *RESPONSIVE TO DESSICATION 22* (*RD22*, AT5G25610), *JASMONATE-ZIM-DOMAIN PROTEIN 6* (*JAZ6*, AT1G72450), and a large number genes belonging to the *MYB*
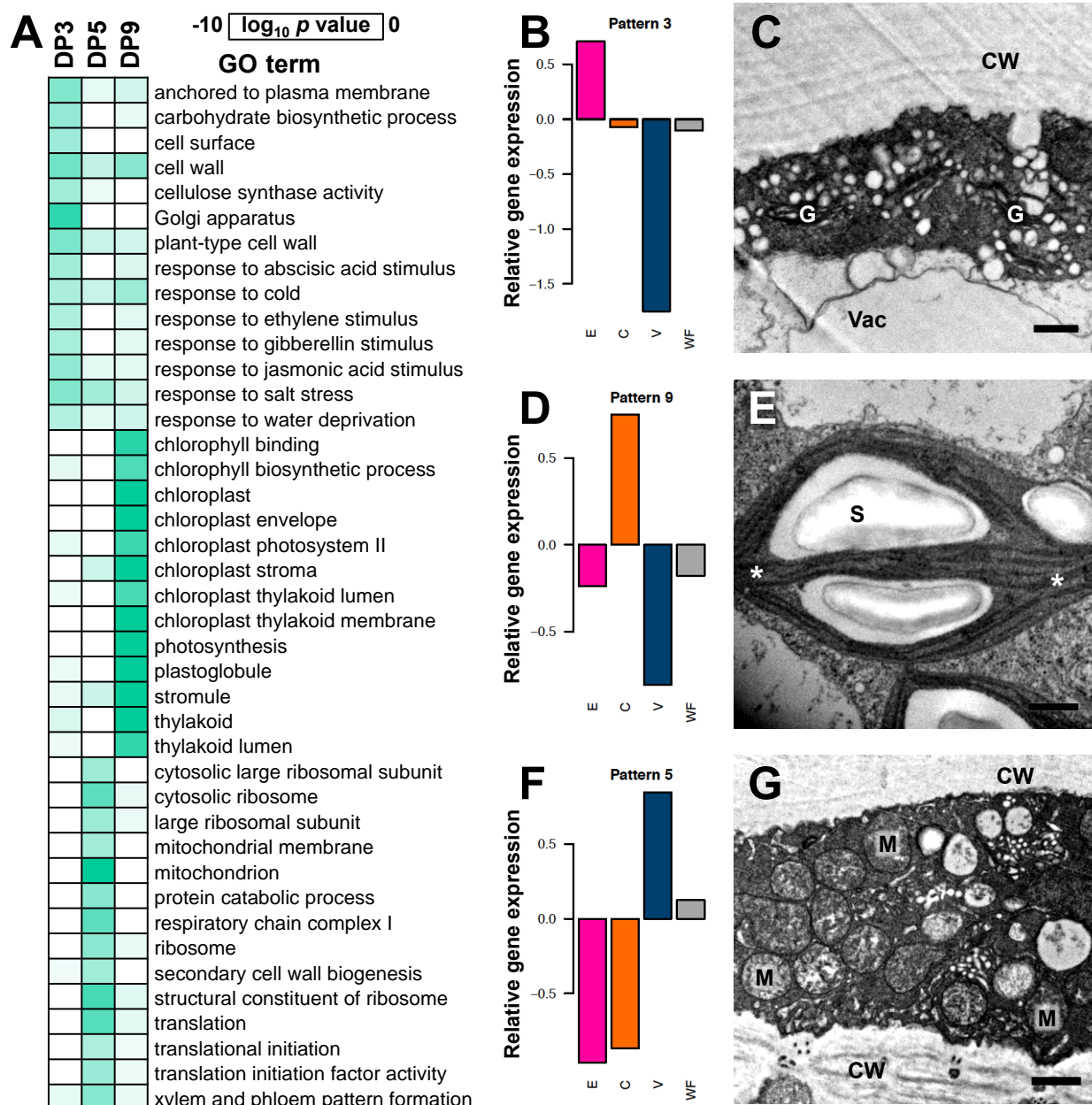
Figure 3.5: Enrichment, clustering, and anatomical analysis of the globular stage canola (*Brassica napus*) funiculus.

A: Heatmap of select gene ontology (GO) terms found using ChipEnrich that are enriched in select dominant patterns (DPs). Increased color opacity indicates greater enrichment (i.e. lower *p* value).

B: Select DP generated by fuzzy *K*-means (FKM) clustering showing high transcript accumulation in the epidermis (E).

C: An epidermal cell showing the outer tangential cell wall (CW), the vacuole (Vac), and numerous Golgi apparatuses (G). Scale bar = 500 nm.

D: Select DP generated by FKM clustering showing high transcript accumulation in the cortex (C).

E: A representative chloroplast from a cortical cell. Thylakoid membranes (*) and starch (S) are present. Scale bar = 400 nm.
F: Select DP generated by FKM clustering showing high transcript accumulation in the vasculature (V).
G: Numerous mitochondria (M) are present in the cells of the vasculature. CW = cell wall. Scale bar = 750 nm.

family (-3, AT1G22640; -15, AT3G23250; -17, AT3G61250; -30, AT3G28910; - 32, AT4G34990; -77, AT3G50060; -94, AT3G47600; -96, AT5G62470).

DP9 shows transcripts that are highly abundant in the cortex (Figure 3.5A, D). The majority of the enriched GO terms found in this pattern are related to the chloroplast and photosynthesis (Figure 3.5A). These GO terms include: chloroplast thylakoid membrane, thylakoid, chloroplast, chloroplast envelope, chloroplast stroma, photosynthesis, plastoglobule, stromule, and chlorophyll biosynthetic process. Among other GO categories related to the chloroplast and photosynthesis, chlorophyll binding, thylakoid lumen, chloroplast photosystem II, and chloroplast thylakoid lumen were all highly enriched only in DP9. Some of the genes belonging to these GO terms are: *PHOTOSYSTEM I SUBUNIT O*, (*PSAO*, AT1G08380), *PHOTOSYSTEM I SUBUNIT D-1* (*PSAD-1*, AT4G02770), *RUBISCO ACTIVASE* (*RCA*, AT2G39730), *LIGHT HARVESTING COMPLEX OF PHOTOSYSTEM II 5* (*LHCB5*, AT4G10340), *PHOTOSYSTEM I SUBUNIT K* (*PSAK*, AT1G30380), *GLYCERALDEHYDE-3-PHOSPHATE DEHYDROGENASE B SUBUNIT* (*GAPB*, AT1G42970), *EARLY LIGHT-INDUCABLE PROTEIN* (ELIP, AT3G22840), and *PHOTOSYSTEM II SUBUNIT P-2* (*PSBP-2*, AT2G30790). Figure 3.5E shows a representative chloroplast of a cortical cell. The structural integrity of the chloroplast, including intact thylakoid membranes, indicates functionality in photosynthetic processes, supporting the GO term enrichment data.

DP5 shows transcript accumulation that is associated with the vascular tissues of the funiculus (Figure 3.5A, F). Many of the GO terms enriched in this pattern appears to be related to protein synthesis (structural constituent of ribosome, translation, cytosolic ribosome, ribosome, cytosolic large ribosomal subunit, protein catabolic process, translation initiation

factor activity, large ribosomal subunit, and translational initiation) and mitochondrial activity (mitochondrion, respiratory chain complex I, and mitochondrial membrane).

HUELLENLOS (*HLL*, AT1G17560), *RIBOSOMAL PROTEIN S6* (*RPS6*, AT4G31700), *RIBOSOMAL PROTEIN L24B* (*RPL24B*, AT3G53020), *RIBOSOMAL PROTEIN L18* (*RPL18*, AT3G05590) and *34* (*RPL34*, AT1G69620), *NUCLEAR FUSION DEFECTIVE 3* (*NFD3*, AT1G31817), *EUKARYOTIC TRANSLATION INITIATION FACTOR 4A1* (*EIF4A1*, AT3G13920), *3A* (*EIF3A*, AT4G11420) and *3K* (*EIF3K*, AT4G33250), *NOVEL CAP-BINDING PROTEIN* (*NCBP*, AT5G18110), and *TRANSLATION INITIATION FACTOR SUBUNIT 3H1* (*TIF3H1*, AT1G10840) are all genes that are found within multiple protein-synthesis related GO terms.

Some examples of genes related to cellular respiration that were found in the GO terms enriched in DP5 include: *MALATE DEHYDROGENASE* (*MDH*, AT3G47520), *SUCCINATE DEHYDROGENASE SUBUNIT 4* (*SDH4*, AT2G46505), *GLYCERALDEHYDE-3-PHOSPHATE DEHYDROGENASE C SUBUNIT* (*GAPC*, AT3G04120), *ISOCITRATE DEHYDROGENASE 1* (*IDH1*, AT4G35260), and *CITRATE SYNTHASE 5* (*CSY5*, AT3G60100). Other genes found in the GO terms were: *MITOCHONDRIAL ACYL CARRIER PROTEIN 2* (*MTACP2*, AT1G65290), *TRANSLOCASE OF THE OUTER MITOCHONDRIAL MEMBRANE 6* (*TOM6*, AT1G49410), *GAMMA CARBONIC ANHYDRASE LIKE 1* (*GAMMA CAL1*, AT5G63510), *GAMMA CARBONIC ANHYDRASE 3* (*GAMMA CA3*, AT5G66510), *EMBRYO DEFECTIVE 1467* (*EMB1467*, AT5G37510), and *CYTOCHROME C OXIDASE 10* (*COX10*, AT2G44520). Figure 3.5G shows a cell from the vascular tissues that is rich in mitochondria, suggesting that the vasculature is a very energy-demanding tissue in the funiculus.

Secondary cell wall biogenesis, and xylem and phloem pattern formation are two other GO terms that were significantly enriched in DP5 (Figure 3.5A). *IRREGULAR XYLEM 14* (*IRX14*, AT4G36890), *NAC SECONDARY WALL THICKENING PROMOTING FACTOR2* (*NST2*, AT3G61910), and *SCARFACE* (*SFC*, AT5G13300) are three genes that were found within these GO terms. As Figure 2.2 shows, xylem and phloem tissues have both increased in the funiculus from the ovule to globular stage, and continue to increase throughout seed development.

Supplementary Datasets

All supplementary files can be provided digitally in .xlsx format upon request.

Supplementary Dataset 1: Gene IDs, transcript lengths, and FPKM values of the bioreplicates of epidermis, cortex, vasculature and whole funiculus samples, as found in the transcript expression file outputted by Cufflinks after alignment of RNA-seq data to the *Brassica napus* genome using TopHat.

Supplementary Dataset 2: List of all detected transcripts (FPKM $\geq$ 1 in at least one sample) in the canola (*Brassica napus*) funiculus vs. the list of transcripts found in the epidermis, cortex, and/or vasculature bioreplicates that were not detected in the whole funiculus bioreplicates. The calculated tissue specificity index (*I*) of each transcript is also presented.

Supplementary Dataset 3: List of genes found in each dominant pattern generated by fuzzy *K*-means clustering of the detected transcript set (FPKM $\geq$ 1 in at least one sample, mean FPKM value used) in the different tissues of the *Brassica napus* funiculus. Both *B. napus* gene names as well as their corresponding AGI IDs are presented.

Supplementary Dataset 4: List of gene ontology terms and their $\log_{10} p$ values as determined using ChipEnrich associated with each dominant pattern of transcript accumulation.

Supplementary Dataset 5: List of genes found in each enriched gene ontology (GO) term (using ChipEnrich) in each dominant pattern. The number of genes belonging to each GO term as well as the *p* value associated with each GO term is also presented.

DISCUSSION

LMD combined with RNA-seq can offer valuable insight into the spatial distribution of transcript accumulation in multicellular systems such as the canola funiculus. LMD enables the selection of specific tissue types and RNA-seq allows for whole transcriptome data to be revealed at an unparalleled resolution. Combining these cutting-edge methods with bioinformatics approaches, I was able to detect novel tissue-specific patterns of transcript accumulation in the canola funiculus, a region of the seed that has not previously been genetically characterized. Anatomical evidence further supports the transcriptome data and reveals the dynamic nature of each tissue system in the funiculus.

1. LASER MICRODISSECTION INCREASES THE SPATIAL RESOLUTION OF TRANSCRIPT ACCUMULATION DATASETS

1.1. LMD allows for the recovery of suitable samples for RNA-seq experiments

Because RNA is the starting material used for amplification and sequencing, it is crucial that RNA quality is preserved, or, where degradation is unavoidable, to select amplification systems that compensate for these limitations so that the sequencing is as efficient as possible. As Tables 3.1-3.4 show, despite the partial degradation that has occurred in the RNA isolated from LMD-collected tissues, suitable libraries were constructed using the Ovation® RNA-Seq System V2 kit and a high percentage of the sequenced reads mapped to the reference genome (Table 3.5).

RNA degradation leads to more fragments of RNA – and therefore more 3' end fragments – in the sample. This is problematic because many amplification methods have been developed that utilize primers designed to initiate amplification of the mRNA at the 3' end, thereby biasing the amplification process (Tariq et al. 2011). However, because the Ovation® kit does not

amplify based on the presence of 3' ends (Kurn et al. 2005), RNA samples with RINs as low as 2.0 can be amplified. The Ovation amplification system uses as low as 1 ng of RNA of starting material, which is an advantage for LMD collected samples, as an input of approximately 1-4 million μm^2 of tissue surface area per sample was necessary to recover an adequate amount of RNA. This is beneficial because LMD, although a valuable technique in obtaining pure tissues, can be somewhat time-consuming because of the small fragment sizes of tissue that can be acquired at one time.

1.2. LMD facilitates the detection of differential transcript accumulation among tissues of the canola funiculus

Schiebold et al. (2011) affirm that LMD is a critical technology in establishing a comprehensive profile of seed development in *Brassica napus*, and that the undertaking of these types of studies will have profound implications in the fields of systems biology as well as biotechnology. LMD permits the physical acquisition of specific tissues of interest that would otherwise be inaccessible. This helps reveal unique transcript accumulation among the tissue systems of the canola funiculus. Despite a similar number of total transcripts, as well as similar levels of lowly, moderately, and highly abundant transcripts appearing in each sample surveyed (Figure 3.3C), just over 23% of those transcripts are tissue-specific (Figure 3.3A, B) and would not have been detected without analyzing each tissue individually.

Belmonte et al. (2013) report a similar phenomenon in their profiling of the transcripts present in the different regions and sub-regions of the Arabidopsis seed: although similar numbers of genes are expressed among the different tissues of the seed, each compartment contains a population of unique mRNAs. This suggests that large sets of genes are quantitatively regulated. Similarly to my results, these authors found that the microdissection of individual

regions revealed additional genes that are not detected when analyzing the entire seed. An additional 2017 genes were found in the microdissected seed regions and sub-regions when compared to the number detected in the whole Arabidopsis seed (Belmonte et al. 2013). From the detected gene sets, these authors were able to assign functions to the different regions and sub-regions of the seed.

2. TISSUE SYSTEMS OF THE CANOLA FUNICULUS EXHIBIT DIFFERENT PATTERNS OF TRANSCRIPT ACCUMULATION

Figure 3.2 shows that the epidermis and cortex group more closely together than any other tissue. The vasculature groups separately from the other two tissue systems, but is most similar to the whole funiculus, likely because it constitutes the largest volume of the funiculus and has the greatest number of cells when compared to the epidermis and cortex. Belmonte et al. (2013) note that transcript accumulation in a particular tissue is strongly correlated to its function. I used GO term enrichment to predict biological processes underlying the development of each of the three tissue systems collected from the canola funiculus. Because each tissue functions in distinct processes, I will address each separately.

2.1. The epidermis functions in cell wall biosynthesis and early programmed cell death

As I have demonstrated previously (Chapter 2), the cell wall of the funiculus epidermis thickens over developmental time. In addition to the compelling anatomical evidence (Figure 2.3), my analysis of GO term enrichment in the epidermis suggests that cell wall enlargement is an important function in this tissue layer. GO terms related to cell wall construction, including cell wall, plant-type cell wall, cellulose synthase activity, and Golgi were all highly enriched in DP3 (Figure 3.5A, B), a pattern of mRNA accumulation particular to the epidermis.

Many of the genes that appear in these GO terms (Supplementary Dataset 5) have known cell

wall modifying functions. For example, *CELLULOSE SYNTHASE 3* encodes an essential

structural component of the transmembrane cellulose synthase complex (Somerville 2006). Burn

et al. (2002) investigated the role of three *CESA* genes (*-1*, *-2*, and *-3*) in Arabidopsis. They

found that *CESA3* antisense lines show an overall reduced plant size as a result of stunted cell

enlargement. Interestingly, leaf pavement cells are also misshapen because of the improper

formation of the cell wall (Burn et al. 2002), suggesting the importance of this gene in forming

epidermal systems.

Other genes found in the enriched GO terms in DP3 include *XYLOGLUCAN*

ENDOTRANSGLUCOSYLASE/HYDROLASE 17 and *TUBULIN ALPHA-6*, both of which also

participate in cell wall development. *XTH* genes encode enzymes that are responsible for

remodeling xyloglucan, a hemicellulose that crosslinks cellulose microfibrils in primary cell

walls (Maris et al. 2009). Reduced *TUA6* activity is associated with aberrant cell wall patterning,

particularly in root hair cells (Bao et al. 2001). *TUA6* encodes the α-tubulin subunit of

microtubules. The microtubule network within plant cells is critical for providing pathways for

the Golgi to traffic components necessary for cell wall growth, including CESA proteins

(Paredez et al. 2006; Crowell et al. 2009). Figure 3.5C confirms cell wall growth occurring via

the action of numerous Golgi apparatuses, and is consistent with what I have already shown to

occur in the globular stage funiculus epidermis (Figure 2.3D, E).

Aside from primary cell wall enlargement, the other major process that appears to be

operating in the epidermis is related to stress responses: GO terms related to response to a

number of abiotic stresses (cold, dehydration, salt) and responses to hormones (abscisic acid,

ethylene, gibberillic acid, and jasmonic acid) are enriched. I have previously shown that the

epidermis undergoes PCD over the course of funiculus development (Chapter 2), characterized

by the breakdown of organelles, vacuolization, and the loss of cytoplasm.

PCD is necessary for the proper development of many maternal seed tissues in many plant

systems. In canola, PCD occurs in several cell layers of the seed coat (Wan et al. 2002).

Similarly to the seed coat, the epidermis likely functions primarily to confer protection to the

delicate and critical internal tissues, without itself being energetically demanding to maintain.

The enrichment of the stress and hormone response GO terms lends further support to this idea

of developmental PCD in the epidermis: abiotic stresses and phytohormones or hormone signal

transduction can promote PCD (Beers and McDowell 2001; Kuriyama and Fukuda 2002; Love et

al. 2008).

Lam (2004) identifies jasmonic acid and ethylene as hormones that induce PCD by

responding to abiotic stress or developmental cues. Response to jasmonic acid stimulus and

response to ethylene stimulus specifically are two GO terms that are enriched in the epidermis

(Figure 3.5A, B). Many of the genes found in these two GO terms (Supplementary Dataset 5)

encode various MYB transcription factors (TFs). Although this family of TFs is associated with

a diverse range of functions in plants, *MYB30* in particular is well-established as a positive

regulator of PCD in Arabidopsis (Agudelo-Romero et al. 2008; Raffaele et al. 2008; Zheng et al.

2012). *MYB30* is responsible for the biosynthesis of very-long-chain fatty acids (VLCFAs)

(Raffaele et al. 2008). Although these VLCFAs can be integrated into epicuticular waxes,

MYB30 is considered a weak regulator of cuticle formation. Rather, it is suspected that the

VLCFAs are involved in stress signaling and ultimately PCD (Raffaele et al. 2008), though no

concrete pathway has been determined.

MYB77 has recently been implicated in PCD in the flower stigmas of *Brassica napus* plants (Sankaranarayanan et al. 2013). Compatible pollination of canola plants leads to the upregulation of *MYB77* and breakdown of the stigma surface papillae cells. This allows for the penetration and nourishment of the growing pollen tube from the pollen grain. *MYB77* is lowly expressed when self- or incompatible pollination occurs and PCD of the stigma is also considerably reduced (Sankaranarayanan et al. 2013). Functional characterization of the MYB77 protein in this system would be necessary to explicitly define its role in PCD of the canola stigma.

The role of MYB TFs in inducing PCD in the canola funiculus epidermis requires further analysis. Identifying mutants defective in the *MYB* genes and observing how these mutations affect epidermis phenotype could determine how MYB TFs participate in funiculus development. It would also be interesting to investigate if more PCD-specific mRNAs accumulate in the epidermis at later stages of development, and if the appearance of these transcripts is correlated with anatomical PCD events.

2.2. The cortex is a center of photosynthetic activity

DP9 shows that many GO terms related to structural components of the chloroplast and photosynthetic machinery are enriched in the cortex (Figure 3.5A, D). Many genes found in DP9, including *PHOTOSYSTEM I SUBUNIT O*, *PHOTOSYSTEM I SUBUNIT D-1*, and *PHOTOSYSTEM I SUBUNIT K*, encode constituents of the photosystem I complex (Jensen et al. 2007). *LIGHT HARVESTING COMPLEX OF PHOTOSYSTEM II 5* (Nelson and Yocum 2006) and *PHOTOSYSTEM II SUBUNIT P-2* (Yi et al. 2009) encode the intrinsic light harvesting protein and extrinsic membrane protein, respectively, of photosystem II.

TEM images reveal the prevalence (Figure 2.4C) and structural integrity (Figure 3.5D) of the chloroplasts in cortical cells of the funiculus. Glucose, which is the end product of

photosynthesis, is a major carbon source that is transported into the internal seed regions for the production of fatty acids (Troncoso-Ponce et al. 2011), suggesting that the capacity of the cortex for photosynthesis may serve in seed filling processes associated with the growth and development of the embryo. Supporting this idea, the final canola seed oil content is reported to be much higher than transcript levels present in the seed should allow (Borisjuk et al. 2013); Therefore, nutrients – or at least the precursors to synthesis those nutrients – must be produced in other tissues and later exported to the rest of the seed. It is most likely that these nutrients originate from the leaves of the plant, but it is also possible that the funiculus has a role in producing nutrients for the seed.

The photosynthesis that occurs in *Brassica napus* seeds contributes to final seed oil content, despite the limited light that reaches the seed (Ruuska et al. 2004). However, although canola seeds can generate their own nutrients, they remain major sinks in the plant. Hua et al. (2012) demonstrated that photosynthesis in the silique wall contributes to seed oil content, particularly in the maturation phase of seed development, and may even be required for seed metabolism. This suggests that maternal tissues associated with the seed can substantially influence seed filling. The cortex of the funiculus, a maternal tissue that is even more proximal to the rest of the seed than the silique wall, offers a target for increasing photosynthetic activity – and, consequently, nutrient accumulation in the seed – at least in the early stages of development (before it degenerates later as shown and described in Chapter 2).

Alternatively, the cortex may be supplying the nutrients necessary to support growth of the internal vascular strand of the funiculus. This is an especially critical function as the vasculature enlarges over developmental time (Chapter 2).

2.3. The vasculature is metabolically active to drive transport processes

In agreement with my earlier results (Figure 2.2, Chapter 2), the vasculature is growing. GO terms such as xylem and phloem pattern formation, and secondary cell wall biogenesis are enriched in DP5, a pattern showing highly abundant transcripts in the vasculature of the funiculus (Figure 3.5A, F). *IRREGULAR XYLEM 14* and *NAC SECONDARY WALL THICKENING PROMOTING FACTOR2* are two genes found within the enriched GO terms of DP5 (Supplementary Dataset 5). *IRX14* functions in establishing the backbone of xylan, a major component of the hemicellulose found in secondary cell walls (Brown et al. 2007). *NST2* is a NAC TF that is responsible for secondary cell wall formation largely in the walls of anthers and pollen grains, though some expression is detected elsewhere in the plant (Mitsuda et al. 2005).

SCARFACE appears in the xylem and phloem pattern formation GO term, and is responsible for vasculature continuity (Sieburth et al. 2006). Loss-of-function mutants exhibit leaves that do not form an interconnected network of veins (Sieburth et al. 2006). As I had previously suggested (Chapter 2), the increased vasculature in the funiculus likely serves in seed filling, particularly in preparation for the maturation phase of seed development, with the xylem allowing for embryo elongation and the phloem allowing for increased nutrient transport.

The majority of the enriched GO terms in the vasculature are related to the mitochondria and ribosomes, suggesting that high metabolic activity is associated with vasculature proliferation. Because some mature cell types of plant vascular tissues, such as tracheary elements of the xylem and sieve tube elements of the phloem (Lough and Lucas 2006), are incapable of transcription, they could not contribute to GO term enrichment. Consequently, the high metabolic activity must be restricted to the non-conducting cell types of the vasculature. Indeed, although tracheary elements are dead and hollow cells, precursor cells producing secondary cell walls during tracheary element differentiation are cytoplasmically dense, with numerous

mitochondria and ribosomes among other organelles (Turner et al. 2007). As well, although sieve tube elements are largely devoid of mitochondria and ribosomes (van Bel 2003; Kragler 2010), their associated companion cells are often characterized by an abundance of these subcellular components (van Bel 2003; Heo et al. 2014).

That ribosome is one of the enriched GO terms in the vasculature is reasonable given that rapidly developing cells must utilize most of its transcription and translation activities to produce rRNAs and ribosomal proteins (Moss et al. 2007; Kim et al. 2014). Many of the genes included in the ribosome GO term encode ribosomal subunits. For example, RIBOSOMAL PROTEIN S6 is a constituent of the ribosomal 40S subunit, and loss-of-function plants show slowed growth and development, including in meristematic regions (Ren et al. 2012). In addition to functioning as a structural protein in the 60S ribosome (Tiruneh et al. 2013), RPL24B has also been demonstrated to be involved in translation reinitiation of genes regulating carpel development (Nishimura et al. 2005). It is evident that a compromise in ribosome structure can lead to defects in the formation of many different plant organs.

Genes found in the mitochondria-related enriched GO terms include many that are involved in energy producing pathways, such as *GLYCERALDEHYDE-3-PHOSPHATE DEHYDROGENASE C SUBUNIT*, which is involved in glycolysis (Igawa et al. 2009). Additionally, GAPC is essential for fertility, and fruit and seed development (Rius et al. 2008), and likely also funiculus development as well. *GAMMA CARBONIC ANHYDRASE 3* is a subunit of the γCA subcomplex of the mitochondrial complex 1 in Arabidopsis (Wang et al. 2012). *GAMMA CARBONIC ANHYDRASE LIKE 1* is another component of the mitochondrial complex I that is specific to plants and is necessary for plant development (Wang et al. 2012).

The enrichment of the mitochondria and ribosome related GO terms suggests that

mitochondria and ribosome biosynthesis is critical in the developing vasculature of the funiculus. The mitochondria and ribosomes are likely functioning in facilitating transport processes. Transport proteins need to be manufactured by ribosomes, and energy, which would be supplied by the mitochondria, is required for active transport. Collectively, it appears that the majority of the genetic programs active in the vasculature function to increase transport capacity in the seed by three methods: i) the generation of new cells, ii) the differentiation of existing pluripotent cells into specific cell types, and iii) provision of the necessary machinery and energy to enable long-distance transport of materials.

3. CONCLUSIONS

This study shows that the canola funiculus is responsible for fundamental biological processes. Processes such as cell wall biosynthesis, photosynthesis, and vascular growth and differentiation allow the different tissue systems of the funiculus to attain specialized functions, which, in turn, likely serve in promoting proper seed development. However, the biological processes identified here were from genes with known *Arabidopsis thaliana* homologues as well as their functions. Identifying the functions of poorly characterized genes might reveal additional biological processes that occur in the funiculus.

My results confirm that mRNA accumulation is spatially regulated in the different tissue systems of the funiculus. However, as I only examined a single stage of development, it would be imperative to investigate how funicular functions evolve over developmental time in response to the changing energetic demands of the seed. A complete spatial-temporal analysis of the transcripts present in the funiculus would enable a much better understanding of the biology of this organ and how it participates in supporting the seed over the course of development.

CONCLUSIONS AND FUTURE DIRECTIONS

The purpose of this research is to investigate seed development through the previously understudied structure, the funiculus. Anatomical examinations of the funiculus over the course of seed development at both a broad histological perspective as well as a more detailed ultrastructural level show that dynamic changes occur in every tissue system at every major stage of seed development. Supporting the anatomical data, transcriptome analysis of the different tissue systems of the funiculus reveals that mRNAs are accumulated in a spatial manner to orchestrate funiculus development. This study reveals that important biological processes occur in the funiculus that are crucial for seed success.

Using the same techniques employed in this project (LMD and RNA-seq), a high-resolution spatial-temporal prolife of funiculus transcript accumulation from the mature ovule to the mature seed stage can be obtained. This would provide scientists with a comprehensive dataset that would be of profound agricultural and economic value, and enable the identification of key genes necessary for seed development and nutrient accumulation. This information would serve as an essential resource for plant biologists and contribute immensely to efforts aimed at engineering genetic varieties of canola crops to optimize seed output and therefore impact the Canadian economy.

REFERENCES

Agudelo-Romero, P., Carbonell, P., de la Iglesia, F., Carrera, J., Rodrigo, G., Jaramillo, A., Pérez-Amador, M.A., and Elena, S.F. 2008. Changes in the gene expression profile of *Arabidopsis thaliana* after infection with *Tobacco etch virus*. Virol J. **5**: 92. doi:10.1186/1743-422X-5-92.

Anders, S., Reyes, A., and Huber, W. 2012. Detecting differential usage of exons from RNA-seq data. Genome Res. **22**(10): 2008-2017. doi:10.1101/gr.133744.111.

Bao, Y., Kost, B., and Chua, N. 2001. Reduced expression of α-tubulin genes in *Arabidopsis thaliana* specifically affects root growth and morphology, root hair development and root gravitropism. Plant J. **28**(2): 145–157. doi:10.1046/j.1365-313X.2001.01142.x.

Becker, M.G., Hsu, S.W., Harada, J.J., and Belmonte, M.F. 2014. Genomic dissection of the seed. Front. Plant Sci. **5**. doi:10.3389/fpls.2014.00464.

Beers, E.P., and McDowell, J.M. 2001. Regulation and execution of programmed cell death in response to pathogens, stress and developmental cues. Curr. Opin. Plant Biol. **4**(6): 561–567. doi:10.1016/S1369-5266(00)00216-8.

Belmonte, M.F., Kirkbride, R.C., Stone, S.L., Pelletier, J.M., Bui, A.Q., Yeung, E.C., Hashimoto, M., Fei, J., Harada, C.M., Munoz, M.D., Le, B.H., Drews, G.N., Brady, S.M.,

Goldberg, R.B., and Harada, J.J. 2013. Comprehensive developmental profiles of gene activity in regions and subregions of the Arabidopsis seed. P. Natl. Acad. Sci. USA. **110**(5): E435–E444. doi:10.1073/pnas.ss11005.

Bennett, E.J., Roberts, J.A., and Wagstaff, C. 2011. The role of the pod in seed development: strategies for manipulating yield. New Phytol. **190**(4): 838–853 doi:10.1111/j.1469-8137.2011.03714.x.

Berger, F. 2003. Endosperm: the crossroad of seed development. Curr. Opin. Plant Biol. **9**: 42–50. doi:10.1016/S1369526602000043.

Borisjuk, L., Neuberger, T., Schwender, J., Heinzel, N., Sunderhaus, S., Fuchs, J., Hay, J.O., Tschiersch, H., Braun, H., Denolf, P., Lambert, B., Jakob, P.M., and Rolletschek, H. 2013. Seed architecture shapes embryo metabolism in oilseed rape. Plant Cell **25**(5): 1625–1640. doi:10.1105/tpc.113.111740.

Brown, D.M, Goubet, F., Wong, V.W., Goodacre, R., Stephens, E., Dupree, P., and Turner, S.R. 2007. Comparison of five xylan synthesis mutants reveals new insight into the mechanisms of xylan synthesis. Plant J. 52: 1154–1168. doi:10.1111/j.1365-313X.2007.03307.x.

Burn, J.E., Hocart, C.H., Birch, R.J., Cork, A.C., and Williamson, R.E. 2002. Functional Analysis of the Cellulose Synthase Genes *CesA1*, *CesA2*, and *CesA3* in Arabidopsis. Plant Physiol. **129**(2): 797–807. doi:10.1104/pp.010931.

Canola Council of Canada. 2013. Available from http://.canolacouncil.org.

Chalhoub, B., Denoeud, F., Liu, S., Parkin, I.A.P., Tang, H., Wang, X., Chiquet, J., Belcram, H., Tong, C., Samans, B., Corréa, M., Da Silva, C., Just, J., Falentin, C., Koh, C.S., Le Clainche, I., Bernard, M., Bento, P., Noel, B., Labadie, K., Alberti, A., Charles, M., Arnaud, D., Guo, H., Daviaud, C., Alamery, S., Jabbari, K., Zhao, M., Edger, P.P., Chelaifa, H., Tack, D., Lasselle, G., Mestiri, I., Schnel, N., Le Paslier, M.C., Fan, G., Renault, V., Bayer, P.E., Golicz, A.A., Manoli, S., Lee, T.H., Thi, V.H.D., Chalabi, S., Hu, Q., Fan, C., Tollenaere, R., Lu, Y., Battail, C., Shen, J., Sidebottom, C.H.D., Wang, X., Canaguier, A., Chauveau, A., Bérard, A., Deniot, G., Guan, M., Liu, Z., Sun, F., Lim, Y.P., Lyons, E., Town, C.D., Bancroft, I., Wang, X., Meng, J., Ma, J., Pires, C., King, G.J., Brunel, D., Delourme, R., Renard, M, Aury, J.M., Adams, K.L., Batley, J., Snowdown, R.J., Tost, J., Edwards, D., Zhou, Y., Hau, W., Sharpe, A.G., Paterson, A.H., Guan, C., and Wincker, P. 2014. Early allopolyploid evolution in the post-Neolithic *Brassica napus* oilseed genome. Science **345**(6199): 950–953. doi:10.1126/science.1253435.

Chapman, L.A., and Goring, D.R. 2010. Pollen-pistil interactions regulating successful fertilization in the Brassicaceae. J. Exp. Bot. **61**(7): 1989–1999. doi:10.1093/jxb/erq021.

Cosgrove, D.J. 2005. Growth of the plant cell wall. Nat. Rev. Mol. Cell Bio. **6:** 850–861. doi:10.1038/nrm1746.

Crowell, E.F., Bischoff, V., Desprez, T., Rolland, A., Stierhof, Y.D., Schumacher, K., Gonneau, M., Höfte, H., and Vernhettes, S. 2009. Pausing of Golgi bodies on microtubules regulates secretion of cellulose synthase complexes in *Arabidopsis*. Plant Cell **21**(4): 1141–1154. doi:10.1105/tpc.108.065334.

Drew, M.C., He, C., and Morgan, P.W. 2000. Programmed cell death and aerenchyma formation in roots. Trends Plant Sci. **5**(3): 123–127. doi:10.1016/S1360-1385(00)01570-3.

Eastmond, P., Koláčná, L., and Rawsthorne, S. 1996. Photosynthesis by developing embryos of oilseed rape (*Brassica napus* L.). J. Exp. Bot. **47**(304): 1763–1769. doi:10.1093/jxb/47.11.1763.

Endo, Y. 2012. Anatomical diversity of funicles in Leguminosae. J. Plant Res. **125**(1): 41–53. doi:10.1007/s10265-011-0404-3.

Endress, P.K. 2011. Angiosperm ovules: diversity, development, evolution. Ann-Bot. London **107**(9): 1465–1489. doi:10.1093/aob/mcr120.

Erdelská, O., and Stintzing, F. 2011. Phytochemical and morphological evaluation of flowers and fruits from *Epiphyllum* hybrids during development. Biologica **66**(5): 821–827. doi:10.2478/s11756-011-0081-7.

Gaffal, K.P., Friedrichs, G.J., and El-Gammal, S. 2007. Ultrastructural evidence for a dual function of the phloem and programmed cell death in the floral nectary of *Digitalis purpurea*. Ann-Bot. London **99**(4): 593–607. doi:10.1093/aob/mcm002.

Ghosh, S., Mahoney, S.R., Penterman, J.N., Peirson, D., and Dumbroff, E.B. 2001. Ultrastructural and biochemical changes in chloroplasts during *Brassica napus* senescence. Plant Physiol. Biochem. **39**(9): 777–784. doi:10.1016/S0981-9428(01)01296-7.

Givan, S.A., Bottoms, C.A., and Spollen, W.G. 2012. Computational analysis of RNA-seq. *In* RNA Abundance Analysis. Humana Press, New York, NY. doi:10.1007/978-1-61779-839-9_16.

Gómez, L.D., Sebastien, B., Gilday, A., Li, Y., and Graham I.A. 2006. Delayed embryo development in the *ARABIDOPSIS TREHALOSE-6-PHOSPHATE SYNTHASE 1* mutant is associated with altered cell wall structure, decreased cell division and starch accumulation. Plant J. **46**: 69–84. doi:10.1111/j.1365-313X.2006.02662.x.

Graeber, K., Nakabayashi, K., Miatton, E., Leubner-Metzger, G., and Soppe, W.J.J. 2012. Molecular mechanisms of seed dormancy. Plant Cell Environ. **35**(10): 1769–1786. doi:10.1111/j.1365-3040.2012.02542.x.

Gutierrez, L., Van Wuytswinkel, O., Castelain, M., and Bellini, C. 2007. Combined networks regulating seed maturation. Trends Plant Sci. **12**(7): 294–300. doi:10.1016/j.tplants.2007.06.003.

Harada, J.J., Belmonte, M.F., and Kwong, R.W. 2010. Plant embryogenesis (zygotic and somatic). *In* Encyclopedia of Life Sciences (ELS). Chichester: John Wiley & Sons, Ltd. pp. 1–13. doi:10.1002/9780470015902.a0002042.pub2.

Haughn, G., and Chaudhury, A. 2005. Genetic analysis of seed coat development in *Arabidopsis*. Trends Plant Sci. **10**(10): 472–477. doi:10.1016/j.tplants.2005.08.005.

Heo, J.O., Roszak, P., Furuta, K.M., and Helariutta, Y. 2014. Phloem development: Current knowledge and future perspectives. Am. J. Botany. 101(9): 1393–1402. doi:10.3732/ajb.1400197.

Hills, M.J. 2004. Control of storage-product synthesis in seeds. Curr. Opin. Plant Biol. **7**: 302–308. doi:10.1016/j.pbi.2004.03.003.

Holdsworth, M.J., Bentsink, L., and Soppe, W.J.J. 2008. Molecular networks regulating Arabidopsis seed maturation, after-ripening, dormancy and germination. New Phytol. **179**(1): 33–54. doi:10.1111/j.1469-8137.2008.02437.x.

Hua, W., Li, R.J., Zhan, G.M., Liu, J., Li, J., Wang, X.F., Liu, G.H., and Wang, H.Z. 2012. Maternal control of seed oil content in *Brassica napus*: the role of silique wall photosynthesis. Plant J. **69**(3): 432–444. doi:10.1111/j.1365-313X.2011.04802.x.

Huang, Y., Chen, L., Wang, L., Vijayan, K., Phan, S., Liu, Z., Wan, L., Ross, A., Xiang, D., Datla, R., Pan, Y., and Zou, J. 2009. Probing the endosperm gene expression landscape in *Brassica napus*. BMC Genomics. **10**(1): 256–275. doi:10.1186/1471-2164-10-256.

Igawa, T., Fujiwara, M., Takahashi, H., Sawasaki, T., Endo, Y., Seki, M., Shinozako, K., Fukao, Y., and Yanagawa, Y. 2009. Isolation and identification of ubiquitin-related proteins from *Arabidopsis* seedlings. J. Exp. Bot. **60**(11): 3067–3073. doi:10.1093/jxb/erp134.

Jensen, P.E., Bassi, R., Boekema, E.J., Dekker, J.P., Jansson, S., Leister, D., Robinson, C., and Scheller, H.V. 2007. Structure, function and regulation of plant photosystem I. BBA-Bioenergetics **1767**(5): 335–352. doi:10.1016/j.bbabio.2007.03.004.

Khan, D., Chan, A., Millar, J.L., Girard, I.J., and Belmonte, M.F. 2014. Predicting transcriptional circuitry underlying seed coat development. Plant Sci. **223**: 146–152. doi:10.1016/j.plantsci.2014.03.016.

Kim, Y.K., Kim, S., Shin, Y.J., Hur, Y.S., Kim, W.Y., Lee, M.S., Cheon, C.I., and Verma, D.P.S. 2014. Ribosomal Protein S6, a Target of Rapamycin, Is Involved in the Regulation of rRNA Genes by Possible Epigenetic Changes in *Arabidopsis*. J. Biol. Chem. **289**(7): 3901–3912. doi:10.1074/jbc.M113.515015.

Kragler, F. 2010. RNA in the phloem: A crisis or a return on investment? Plant Sci. **178**(2): 99–104. doi:10.1016/j.plantsci.2009.12.006.

Kuriyama, H., and Fukuda, H. 2002. Developmental programmed cell death in plants. Curr. Opin Plant Biol. 5(6), 568–573. doi:10.1016/S1369-5266(02)00305-9.

Kurn, N., Chen, P., Heath, J.D., Kopf-sill, A., Stephens, K.M., and Wang, S. 2005. Novel isothermal, linear nucleic acid amplification systems for highly multiplexed applications. Clin. Chem. **51**(10): 1973–1981. doi:10.1373/clinchem.2005.053694.

Lagaert, S., Beliën, T., and Volckaert, G. 2009. Plant cell walls: protecting the barrier from degradation by microbial enzymes. Semin. Cell. Dev. Biol. **20**(9): 1064–1073. doi:10.1016/j.semcdb.2009.05.008.

Lam, E. 2004. Controlled cell death, plant survival and development. Nat. Rev. Mol. Cell Bio. **5**(4): 305–315. doi:10.1038/nrm1358.

Li, F., and Viestra, R.D. 2012. Autophagy: a multifaceted intracellular system for bulk and selective recycling. Trends Plant Sci. **17**(9): 526-537. doi: 10.1016/j.tplants.2012.05.006.

Lough, T.J., and Lucas, W.J. 2006. Integrative plant biology: role of phloem long-distance macromolecular trafficking. Annu. Rev. Plant Biol. **57**: 203–232. doi:10.1146/annurev.arplant.56.032604.144145.

Love, A.J., Milner, J.J., and Sadanandom, A. 2008. Timing is everything: regulatory overlap in

plant cell death. Trends Plant Sci. **13**(11), 589–595. doi:10.1016/j.tplants.2008.08.006.

Lucas, P.W., Turner, I.M., Dominy, N.J., and Yamashita, N. 2000. Mechanical defences to herbivory. Ann-Bot. London **86**(5): 913–920. doi:10.1006/anbo.2000.1261.

Maris, A., Suslov, D., Fry, S.C., Verbelen, J.P., and Vissenberg, K. 2009. Enzymic characterization of two recombinant xyloglucan endotransglucosylase/hydrolase (XTH) proteins of *Arabidopsis* and their effect on root growth and cell wall extension. J. Exp. Bot. **60**(13): 3959–3972. doi:10.1093/jxb/erp229.

Mawson, B.T., Steghaus, A.K., and Yeung, E.C. 1994. Structural development and respiratory activity of the funiculus during bean seed (*Phaseolus vulgaris* L.) maturation. Ann-Bot. London **74**(6): 587–594. doi:10.1006/anbo.1994.1158.

McGettigan, P.A. 2013. Transcriptomics in the RNA-seq era. Curr. Opin. Chem. Biol. **17**(1): 4–11. doi:10.1016/j.cbpa.2012.12.008.

Mitsuda, N., Seki, M., Shinozaki, K., and Ohme-Takagi, M. 2005. The NAC transcription factors NST1 and NST2 of *Arabidopsis* regulate secondary wall thickenings and are required for anther dehiscence. Plant Cell **17**(11): 2993–3006. doi:10.1105/tpc.105.036004.

Mordhorst, A.P., Toonen, M.A.J., and de Vries, S.C. 1997. Plant Embryogenesis. Critical Reviews in Plant Sciences, **16**(6): 535–576. doi:10.1080/07352689709701959.

Moss, T., Langlois, F., Gagnon-Kugler, T., and Stefanovsky, V. 2007 A housekeeper with power of attorney: the rRNA genes in ribosome biogenesis. Cell. Mol. Life Sci. **64**(1): 29–49. doi:10.1007/s00018-006-6278-1.

Nelson, T., Tausta, S.L., Gandotra, N., and Liu, T. 2006. Laser microdissection of plant tissue: what you see is what you get. Annu. Rev. Plant Biol. **57**: 181–201. doi:10.1146/annurev.arplant.56.032604.144138.

Nelson, N., and Yocum, C.F. 2006. Structure and function of photosystems I and II. Annu. Rev. Plant Biol. **57**: 521–565. doi:10.1146/annurev.arplant.57.032905.105350.

Ning, S., Wang, L., and Song, Y. 2002. Identification of programmed cell death *in situ* in individual plant cells *in vivo* using a chromosome preparation technique. J. Exp. Bot. **53**(369): 651–658. doi:10.1093/jexbot/53.369.651.

Nishimura, T., Wada, T., Yamamoto, K.T., and Okada, K. 2005. The *Arabidopsis* STV1 protein, responsible for translation reinitiation, is required for auxin-mediated gynoecium patterning. Plant Cell **17**(11): 2940–2953. doi:10.1105/tpc.105.036533.

Oliveros, J.C. 2007. VENNY. An interactive tool for comparing lists with Venn Diagrams. http://bioinfogp.cnb.csic.es/tools/venny/index.html.

Paredez, A.R., Somerville, C.R., and Ehrhardt, D.W. 2006. Visualization of cellulose synthase demonstrates functional association with microtubules. Science **312**(5779): 1491–1495. doi:10.1126/science.1126551.

Pop, M., and Salzberg, S.L. 2008. Bioinformatics challenges of new sequencing technology. Trends Genet. **24**(3): 142–149. doi:10.1016/j.tig.2007.12.006.

Quail, M.A., Gu, Y., Swerdlow, H., and Mayho, M. 2012. Evaluation and optimisation of preparative semi-automated electrophoresis systems for Illumina library preparation. Electrophoresis **33**(23): 3521–3528. doi:10.1002/elps.201200128.

Raffaele, S., Vailleau, F., Léger, A., Joubès, J., Miersch, O., Huard, C., Blée, E., Mongrand, S., Domergue, F., and Roby, D. (2008). A MYB transcription factor regulates very-long-chain fatty acid biosynthesis for activation of the hypersensitive cell death response in *Arabidopsis*. Plant Cell **20**(3), 752–767. doi:10.1105/tpc.107.054858.

Ramsay, N.A., Glover, B.J. 2005. MYB-bHLH-WD40 protein complex and the evolution of cellular diversity. Trends Plant Sci. **10**: 63–70. doi:10.1016/j.tplants.2004.12.011.

Ramsköld, D., Kavak, E., and Sandberg, R. 2012. How to analyze gene expression using RNA-sequencing data. *In* Next Generation Microarray Bioinformatics. Humana Press, New York, NY. doi:10.1007/978-1-61779-400-1_17.

Ren, M., Venglat, P., Qiu, S., Feng, L., Cao, Y., Wang, E., Xiang, D., Wang, J., Alexander, D., Chalivendra, S., Mattoo, A., Selvaraj, G., and Datla, R. 2012. Target of rapamycin signaling regulates metabolism, growth, and life span in *Arabidopsis*. Plant Cell **24**(12): 4850–4874. doi:10.1105/tpc.112.107144.

Roberts, A., Pimentel, H., Trapnell, C., and Pachter, L. 2011. Identification of novel transcripts in annotated genomes using RNA-Seq. Bioinformatics **27**(17): 2325–2329. doi:10.1093/bioinformatics/btr355.

Rius, S.P., Casati, P., Iglesias, A.A., and Gomez-Casati, D.F. 2008. Characterization of Arabidopsis lines deficient in GAPC-1, a cytosolic NAD-dependent glyceraldehyde-3-phosphate dehydrogenase. Plant Physiol. **148**(3): 1655–1667. doi:10.1104/pp.108.128769.

Ruuska, S.A., Schwender, J., and Ohlrogge, J.B. 2004. The capacity of green oilseeds to utilize photosynthesis to drive biosynthetic processes. Plant Physiol. **136**(1): 2700–2709. doi:10.1104/pp.104.047977.

Sankaranarayanan, S., Jamshed, M., Deb, S., Chatfield-Reed, K., Kwon, E.J.G., Chua, G., and Samuel, M.A. 2013. Deciphering the stigmatic transcriptional landscape of compatible and self-incompatible pollinations in *Brassica napus* reveals a rapid stigma senescence response following compatible pollination. Mol. Plant sst066. doi:10.1093/mp/sst066.

Schiebold, S., Tschiersch, H., Borisjuk, L., Heinzel, N., Radchuk, R., and Rolletschek, H. 2011. A novel procedure for the quantitative analysis of metabolites, storage products and transcripts of laser microdissected seed tissues of Brassica napus. Plant Methods 7(1): 19. doi:10.1186/1746-4811-7-19.

Schroeder, A., Mueller, O., Stocker, S., Salowsky, R., Leiber, M., Gassmann, M., Lightfoot, S., Menzel, W., Granzow, M., and Ragg, T. 2006. The RIN: an RNA integrity number for assigning integrity values to RNA measurements. BMC Mol. Biol. **7**(1): 3–17. doi:10.1186/1471-2199-7-3.

Sieburth, L.E., Muday, G.K., King, E.J., Benton, G., Kim, S., Metcalf, K.E., Meyers, L., Seamen, E., and Van Norman, J.M. 2006. *SCARFACE* encodes an ARF-GAP that is required for normal auxin efflux and vein patterning in *Arabidopsis*. Plant Cell **18**(6): 1396–1411. doi:10.1105/tpc.105.039008.

Somerville, C. 2006. Cellulose synthesis in higher plants. Annu. Rev. Cell Dev. Biol. **22**: 53–78. doi:10.1146/annurev.cellbio.22.022206.160206.

Stadler, R., Lauterbach, C., and Sauer, N. 2005. Cell-to-cell movement of green fluorescent protein reveals post-phloem transport in the outer integument and identifies symplastic domains in Arabidopsis seeds and embryos. Plant Physiol. **139**: 701–712. doi:10.1104/pp.105.065607.

Steeves, T.A., and Sussex, I.M. 1996. Differentiation of the plant body: the elaboration of pattern. *In* Patterns in plant development, 2nd ed. Cambridge University Press, New York, NY.

Szymanski, D.B., and Cosgrove, D.J. 2009. Dynamic coordination of cytoskeletal and cell wall systems during plant cell morphogenesis. Curr. Biol. **19**(17): R800–R811. doi:10.1016/j.cub.2009.07.056.

Tangrea, M.A., Chuaqui, R.F., Gillespie, J.W., Ahram, M., Gannot, G., Wallis, B.S., Best, C.J.M., Linehan, W.M., Liotta, L.A., Pohida, T.J., Bonner, R.F., and Emmert-Buck, M.R. 2004. Expression microdissection: operator-independent retrieval of cells for molecular profiling. Diagn. Mol. Pathol. **13**(4): 207–212.

Tari, L., Baral, C., and Kim, S. 2009. Fuzzy c-means clustering with prior biological knowledge. J. Biomed. Inform. **42**(1): 74–81. doi:10.1016/j.jbi.2008.05.009.

Tariq, M.A., Kim, H.J., Jejelowo, O., and Pourmand, N. 2011. Whole-transcriptome RNAseq analysis from minute amount of total RNA. Nucleic Acids Res. **39**(18): E120-130. doi:10.1093/nar/gkr547.

Tiruneh, B.S., Kim, B.H., Gallie, D.R., Roy, B., and von Arnim, A.G. 2013. The global translation profile in a ribosomal protein mutant resembles that of an eIF3 mutant. BMC Biol. **11**(1): 123. doi:10.1186/1741-7007-11-123.

Tong, C., Wang, X., Yu, J., Wu, J., Li, W., Huang, J., Dong, C., Hua, W., and Liu, S. 2013. Comprehensive analysis of RNA-seq data reveals the complexity of the transcriptome in *Brassica rapa*. BMC Genomics **14**(1): 689. doi:10.1186/1471-2164-14-689.

Trapnell, C., Pachter, L., and Salzberg, S.L. 2011. TopHat: discovering splice junctions with RNA-Seq. Bioinformatics **25**(9): 1105–1111. doi:10.1093/bioinformatics/btp120.

Trapnell, C., Roberts, A., Goff, L., Pertea, G., Kim, D., Kelley, D.R., Pimentel, H., Salzberg, S.L., Rinn, J.L., and Pachter, L. 2012. Differential gene and transcript expression analysis of RNA-seq experiments with TopHat and Cufflinks. Nat. Protoc. **7**(3): 562–578. doi:10.1038/nprot.2012.016.

Troncoso-Ponce, M.A., Kilaru, A., Cao, X., Durrett, T.P., Fan, J., Jensen, J. K., Thrower, N.A., Pauly, M., Wilkerson, C., and Ohlrogge, J.B. 2011. Comparative deep transcriptional profiling of four developing oilseeds. Plant J. **68**(6): 1014–1027. doi: 10.1111/j.1365-313X.2011.04751.x

Turner, S., Gallois, P., and Brown, D. 2007. Tracheary element differentiation. Annu. Rev. Plant Biol. **58**: 407–433. doi:10.1146/annurev.arplant.57.032905.105236.

van Bel, A.J. 2003. The phloem, a miracle of ingenuity. Plant Cell Environ. **26**(1): 125–149. doi: 10.1046/j.1365-3040.2003.00963.x.

van Doorn, W.G. and Woltering, E.J. 2005. Many ways to exit? Cell death categories in plants. Trends Plant Sci. **10**(3): 117–122. doi:10.1016/j.tplants.2005.01.006.

van Doorn, W.G., Beers, E.P., Dangl, J.L., Franklin-Tong, V.E., Gallois, P., Hara-Nishimura, I., Jones, A.M., Kawai-Yamada, M., Lam, E., Mundy, J., Mur, L.A.J., Petersen, M., Smertenko, A., Taliansky, M., Van Breusegem, F., Wolper, T., Woltering, E., Zhivotovsky, B., and Bozhkov, P.V. 2011. Morphological classification of plant cell deaths. Cell Death Differ. **18**(8): 1241–1246. doi:10.1038/cdd.2011.36.

Vianello, A., Zancani, M., Peresson, C., Petrussa, E., Casolo, V., Krajňáková, Patui, S, Braidot, E., and Macri, F. 2007. Plant mitochondrial pathway leading to programmed cell death. Physiol. Plantarum **129**(1): 242–252. doi:10.1111/j.1399-3054.2006.00767.x.

Wan, L., Xia, Q., Qiu, X., and Selvaraj, G. 2002. Early stages of seed development in *Brassica napus*: a seed coat-specific cysteine proteinase associated with programmed cell death of the inner integument. Plant J. **30**(1): 1–10. doi: 10.1046/j.1365-313X.2002.01262.x.

Wang, Z., Gerstein, M., and Snyder, M. 2009. RNA-Seq: a revolutionary tool for transcriptomics. Nat. Rev. Genet. **10**(1): 57–63. doi:10.1038/nrg2484.

Wang, Q., Fristedt, R., Yu, X., Chen, Z., Liu, H., Lee, Y., Guo, H., Merchant, S.S., and Lin, C. 2012. The γ-carbonic anhydrase subcomplex of mitochondrial complex I is essential for

development and important for photomorphogenesis of Arabidopsis. Plant Physiol. **160**(3): 1373–1383. doi:10.1104/pp.112.204339.

Weselake, R.J., Taylor, D.C., Rahman, M.H., Shah, S., Laroche, A., McVetty, P.B.E., and Harwood, J. L. 2009. Increasing the flow of carbon into seed oil. Biotechnol. Adv. **27**(6): 866–878. doi:10.1016/j.biotechadv.2009.07.001.

Yanai, I., Benjamin, H., Shmoish, M., Chalifa-Caspi, V., Shklar, M., Ophir, R., Bar-Even, A., Horn-Saban, S., Safran, M., Domany, E., Lancet, D., and Shmueli, O. 2005. Genome-wide midrange transcription profiles reveal expression level relationships in human tissue specification. Bioinformatics **21**(5): 650–659. doi: 10.1093/bioinformatics/bti042.

Yeung, E.C. and Saxena, P.K. 2005. Histological techniques. *In* Protocols for Somatic Embryogenesis in Woody Plants. *Edited by* S.M. Jain and P.K. Gupta. Springer, Netherlands. pp. 517–537.

Yi, X., Hargett, S.R., Frankel, L.K., and Bricker, T.M. 2009. The PsbP protein, but not the PsbQ protein, is required for normal thylakoid architecture in *Arabidopsis thaliana*. FEBS Lett. **583**(12): 2142–2147. doi:10.1016/j.febslet.2009.05.048.

Yu, B., Gruber, M., Khachatourians, G.G., Hegedus, D.D., and Hannoufa, A. 2010. Gene expression profiling of developing *Brassica napus* seed in relation to changes in major storage compounds. Plant Sci. **178**(4): 381–389. doi: 10.1016/j.plantsci.2010.02.007.

Zhang, C., Barthelson, R.A., Lambert, G.M., and Galbraith, D.W. 2008. Global characterization of cell-specific gene expression through fluorescence-activated sorting of nuclei. Plant Physiol. **147**(1): 30–40. doi:10.1104/pp.107.115246.

Zheng, Y., Schumaker, K.S., and Guo, Y. 2012. Sumoylation of transcription factor MYB30 by the small ubiquitin-like modifier E3 ligase SIZ1 mediates abscisic acid response in *Arabidopsis thaliana*. P. Natl. Acad. Sci. USA **109**(31): 12822–12827. doi:10.1073/pnas.1202630109.